

# Identification of meteorite source regions in the Solar System

Mikael Granvik<sup>a,b,\*</sup>, Peter Brown<sup>c,d</sup>

<sup>a</sup>*Department of Physics, P.O. Box 64, 00014 University of Helsinki, Finland*

<sup>b</sup>*Department of Computer Science, Electrical and Space Engineering, Luleå University of Technology, Box 848, S-98128 Kiruna, Sweden*

<sup>c</sup>*Department of Physics and Astronomy, University of Western Ontario, N6A 3K7, London, Canada*

<sup>d</sup>*Centre for Planetary Science and Exploration, University of Western Ontario, N6A 5B7, London, Canada*

---

## Abstract

Over the past decade there has been a large increase in the number of automated camera networks that monitor the sky for fireballs. One of the goals of these networks is to provide the necessary information for linking meteorites to their pre-impact, heliocentric orbits and ultimately to their source regions in the solar system. We re-compute heliocentric orbits for the 25 meteorite falls published to date from original data sources. Using these orbits, we constrain their most likely escape routes from the main asteroid belt and the cometary region by utilizing a state-of-the-art orbit model of the near-Earth-object population, which includes a size-dependence in delivery efficiency. While we find that our general results for escape routes are comparable to previous work, the role of trajectory measurement uncertainty in escape-route identification is explored for the first time. Moreover, our improved size-dependent delivery model substantially changes likely escape routes for several meteorite falls, most notably Tagish Lake which seems unlikely to have originated in the outer main belt as previously suggested. We find that reducing the uncertainty of fireball velocity measurements below  $\sim 0.1$  km/s does not lead to reduced uncertainties in the identification of their escape routes from the asteroid belt and, further, their ultimate source regions. This analysis suggests that camera networks should be optimized for the largest possible number of meteorite recoveries with measured speed precisions of order 0.1 km/s.

**Keywords:** Meteorites, Meteors, Asteroids, Comets, Orbit determination

---

## 1. Introduction

Understanding meteorite source regions in the solar system is one of the central problems in contemporary planetary science. Association of certain meteorite classes with families of asteroids or specific asteroids based on commonalities in their reflectance spectra is one approach to bridging the asteroid-meteorite divide (Binzel et al., 2015). As meteorites are delivered to the Earth through a long process of stochastic gravitational and radiative perturbations (Morbidelli and Gladman, 1998), the orbit immediately prior to impact loses memory of its original, specific parent body. However, delivery from the main asteroid belt is sufficiently rapid and well-understood, that statistical inferences as to the source region for meteorite classes may be possible if pre-atmospheric orbits for enough meteorites are measured, a process which has been understood for some time (Wetherill, 1985; Wisdom, 2017). To date roughly two dozen meteorite falls have had orbits measured (Borovička et al., 2015a).

The importance of measuring large numbers of meteorite orbits has motivated development of a new generation of all-sky fireball networks whose primary goal is the instrumental recording of meteorite producing fireballs (Howie et al., 2017; Spurný et al., 2007; Colas, 2016).

An outstanding question for such fireball networks is the precision needed in measurement to meaningfully associate a given meteorite orbit with potential source regions. Clearly the smaller the measurement uncertainty the better, but at what point do reduced uncertainties no longer improve the accuracy of statistical associations with meteorite source regions? Also, what are the limitations on this inversion process imposed by the assumptions of the delivery model?

In this work we have two goals. First, we aim to examine the currently known two dozen meteorite orbits and apply a new near-Earth object (NEO) model which has a size dependence (Granvik et al., 2016) to estimate the probable escape/entrance routes/regions (ER) from, primarily, the main asteroid belt for different meteorite classes. This is the necessary first step in trying to ultimately associate meteorites to original parent bodies, generally presumed to be associated with asteroid collisional families. Secondly, we use the database of two dozen meteorite orbits to examine the role measurement errors, particularly in speed, play in the orbital uncertainty and propagate this through the ER model of Granvik et al. (2016). We hope to gain quantitative insight into the corresponding source region uncertainties. This in turn will provide operational guidance to those building new fireball networks as to the required velocity measurement precision for mete-

---

\*Corresponding author, mgranvik@iki.fi

orite dropping fireballs needed to make meaningful source region identifications.

## 2. Methods

### 2.1. Computation of meteorite orbits

Our computation of the pre-atmospheric heliocentric orbit and associated uncertainties for meteorite falls follows well-established algorithms used to convert apparent meteor trajectories to orbits (Ceplecha, 1987). The method has been validated through comparison with independent numerical approaches (Clark and Wiegert, 2011). The essence of the algorithm is to use an in-atmosphere local trajectory for a fireball and then translate this to an equivalent heliocentric orbit. Here we take the trajectories reported in various literature sources and transform the measured Right Ascension (RA) and Declination (Dec) of an apparent radiant and the measured speed  $v_\infty$  to the initial state vector. We assume that the average speed  $\bar{v} = v_\infty - 1.0 \text{ km s}^{-1}$ . The nominal uncertainties on all measured quantities are also taken from published sources when available. The Meteor Toolkit (Dmitriev et al., 2015), the only open-source implementation of meteor orbit computation software as far as we know, would have been an alternative to our in-house orbit computation software. As it produces very similar results to the technique based on Ceplecha (1987), which was also used in the majority of the fireball producing meteorite fall studies published to date, we chose to remain with that original software.

A major systematic uncertainty in all meteorite computed orbits is the correction applied for pre-luminous flight deceleration. For most published meteorite orbits, insufficient information is provided in the original references to compute this correction or even determine if it has been applied to the final orbital elements. We do not explore this correction further, but merely emphasize that for those studies which do not model the meteoroid entry, the apparent initial speed may be underestimated by of order a few tens of meters per second in some extreme cases.

### 2.2. Prediction of meteorite escape routes

A key ingredient for predicting a meteoroid's likely source region in the solar system is a model describing NEO orbit and size distributions (Granvik et al., 2016). The model also provides probabilistic information about NEO ERs as a function of semimajor axis  $a$ , eccentricity  $e$ , inclination  $i$  and the absolute magnitude  $H$  for NEOs with  $17 < H < 25$ . The  $H$  range corresponds to a diameter  $35 \text{ m} \lesssim D \lesssim 1400 \text{ m}$  when assuming an average geometric albedo  $p_V = 0.14$  (Pravec et al., 2012). The model accounts for 7 different ERs in the solar system: Hungaria asteroids, Phocaea asteroids and Jupiter-family comets as well as asteroids escaping through the  $\nu_6$  secular resonance or the 3:1J, 5:2J and 2:1J mean-motion resonances (MMR) with Jupiter. We note that less important

yet non-negligible escape routes have been incorporated into the adjacent main resonances.

When neglecting correlations between orbital elements derived from a meteoroid trajectory, the probability for a meteoroid with orbital elements and corresponding uncertainties ( $a \pm \delta a, e \pm \delta e, i \pm \delta i$ ) to originate in ER  $s$  is

$$p_s(a, e, i, \delta a, \delta e, \delta i) = \frac{\int_{a-\delta a}^{a+\delta a} \int_{e-\delta e}^{e+\delta e} \int_{i-\delta i}^{i+\delta i} \int_{H=17}^{25} N_s(a, e, i, H) da de di dH}{\sum_s \int_{a-\delta a}^{a+\delta a} \int_{e-\delta e}^{e+\delta e} \int_{i-\delta i}^{i+\delta i} \int_{H=17}^{25} N_s(a, e, i, H) da de di dH}, \quad (1)$$

where  $N_s(a, e, i, H)$  is the debiased differential number distribution of NEOs originating in ER  $s$ . So in essence the probability is the ratio of the number of asteroids on the specified orbit originating in ER  $s$  and the total number of asteroids on the specified orbit. In practice,  $N_s(a, e, i, H)$  is discretized with bin sizes ( $\Delta a, \Delta e, \Delta i, \Delta H$ ) and used as a four-dimensional look-up table. In what follows Eq. 1 is therefore approximated as

$$p_s(a, e, i, \delta a, \delta e, \delta i, \Delta a, \Delta e, \Delta i) = \frac{\sum_{j=j_{\min}}^{j_{\max}} \sum_{k=k_{\min}}^{k_{\max}} \sum_{l=l_{\min}}^{l_{\max}} \sum_{m=1}^M N_s(a_j, e_k, i_l, H_m)}{\sum_{s=1}^7 \sum_{j=j_{\min}}^{j_{\max}} \sum_{k=k_{\min}}^{k_{\max}} \sum_{l=l_{\min}}^{l_{\max}} \sum_{m=1}^M N_s(a_j, e_k, i_l, H_m)}, \quad (2)$$

where the summation over  $s$  is over all 7 ERs and the summation over  $m$  is over all  $M$   $H$  bins available. The limits for the summation over  $j$  are defined as

$$j_{\min} = \begin{cases} \lceil \frac{a-\delta a-a_{\min}}{\Delta a} \rceil & \text{when } a_{\min} < a - \delta a, \\ 1 & \text{when } a_{\min} \geq a - \delta a. \end{cases}$$

$$j_{\max} = \begin{cases} 0 & \text{when } a_{\min} > a + \delta a, \\ \lceil \frac{a+\delta a-a_{\min}}{\Delta a} \rceil & \text{when } a_{\min} < a + \delta a < a_{\max}, \\ J & \text{when } a_{\max} \leq a + \delta a. \end{cases}$$

where  $a_{\min}$  and  $a_{\max}$  are the minimum and maximum semimajor axes covered by the model, respectively,  $J$  is the number of semimajor axis bins in the discretized model, and  $\lceil x \rceil$  denotes the ceiling of  $x$ . The limits for  $k$  and  $l$  are obtained by replacing ( $j_{\min}, j_{\max}, a, \delta a, a_{\min}, a_{\max}, \Delta a, J$ ) with ( $k_{\min}, k_{\max}, e, \delta e, e_{\min}, e_{\max}, \Delta e, K$ ) and ( $l_{\min}, l_{\max}, i, \delta i, i_{\min}, i_{\max}, \Delta i, L$ ), respectively.

The model by Granvik et al. (2016) is bounded by  $a_{\min} = 0.3 \text{ au}$ ,  $a_{\max} = 4.2 \text{ au}$ ,  $e_{\min} = 0$ ,  $e_{\max} = 1$ ,  $i_{\min} = 0^\circ$ , and  $i_{\max} = 180^\circ$ . Note that Granvik et al. (2016) did not force  $a_{\min} = 0.3 \text{ au}$ , but this is a naturally occurring lower limit caused by the fact that there does not exist a mechanism to decouple an asteroid's orbit from that of Mercury. In terms of the resolution ( $\Delta a, \Delta e, \Delta i$ ) we here use both low resolution ( $0.1 \text{ au}, 0.04, 4^\circ$ ) and high resolution ( $0.05 \text{ au}, 0.02, 2^\circ$ ).

As with the NEO model of Bottke et al. (2002), the calculation assumes that the meteoroid orbit is similar to the orbit of its asteroidal (or cometary) parent body and the estimate for the source region applies, strictly speaking, to that parent body. We emphasize that, although large objects affect  $p_s$ , this value is primarily driven by the smallest objects included in the NEO model, that is, those with diameters of a few tens of meters or so, due to the steep NEO size distribution.

### 3. Data

We collected the observed trajectories as well as meteorite classifications, densities, and cosmic-ray exposure ages (the latter three collectively called geophysical data hereafter) for known fireball-producing meteorite falls from the literature (Tables 1 and 2). The list of meteorite falls should be complete less a few recent and as of yet unpublished events. All meteorite-producing fireballs with orbits that we have used have trajectories and speeds computed using some combination of instrumental records, including dedicated camera networks, calibrated casual video recordings, seismic, infrasound, satellite or pre-atmospheric telescopic detection. Details of the nature of each event and quality of the resulting orbits is discussed in Borovička et al. (2015a). We have extracted from the original published reference for each event (all primary references are listed in Tables 1) the local trajectory and corresponding quoted uncertainties, and then independently computed orbits for consistency.

## 4. Results and discussion

### 4.1. Orbits of known meteorite falls

We recomputed the orbits of known meteorite falls based on the observational data presented in Sect. 3, using the original information from literature sources as much as possible. In some cases we could not independently match the published orbit with the radiant and speed given in the same reference. In those cases we have tried to use the original trajectory information (and stated errors) as much as possible to recompute the orbit from fundamental measurements and propagate the uncertainties through to a final geocentric radiant and orbit. Where this was not possible, we match the geocentric radiant and geocentric velocity as published to produce the final orbital elements, even if the final orbits differ slightly from published values. In most cases these systematic differences are much smaller than the formal uncertainties. In some cases, quoted errors represent only the uncertainty in the mathematical model fit in the trajectory solution to data. This ignores other uncertainties in the system such as centroid pick errors or differences in calibration precision within the image as well as model assumptions of the fit.

These differences are often due to ambiguities in the original reference, such as whether apparent radiants refer

to the beginning of the trajectory or the mid-point (or end). We assume where this is not stated that apparent radiants are computed for the beginning of the fireball.

In Table 1 we refer to an "equivalent" radiant and/or speed which produces the literature values of the original apparent trajectory or geocentric radiant/geocentric velocity. The final orbits are then found using our adopted corrections as described above.

The resulting orbits are similar to typical NEO orbits with 20 falls having nominal semimajor axes inside the 3:1J mean-motion resonance (MMR) with Jupiter (J) and the remaining four having nominal semimajor axes suggesting an origin in the outer main belt exterior to the 3:1J MMR but inside the 5:2J MMR (Table 3). The  $1\text{-}\sigma$  uncertainty on the semimajor axis is typically  $\delta a < 0.05$  au but for the C and CM meteorite falls the uncertainty is  $\delta a \sim 0.3$  au which immediately suggests that the ER for C and CM meteorites cannot be accurately determined. The other elements are well-constrained less two falls with essentially unconstrained longitude of ascending node and argument of perihelion due to near zero-inclination orbits.

Our recomputed orbits are generally in statistical agreement with those reported in the original literature sources. However, some meteorite orbits do show noticeable differences; for example in cases where complete initial state vector information (like apparent radiant) are omitted (such as Lost City and Annama). In other cases, these differences are due to the low inclination of the orbits (e.g., Maribo and Villalbeto de la Peña) where small differences in corrections will make large differences to the angular elements. For Chelyabinsk, we have two independent literature estimates of the original orbit and a low inclination which makes our independent recomputed orbital elements differ slightly from both literature values. We have chosen to use our recomputed values using uniform corrections (like average speed) recognizing there may remain small systematic uncertainties due to lack of consistency in reported state vector quantities. This is in addition to quality differences resulting from the techniques used to make trajectory measurements (cf. Borovička et al., 2015a).

None of the meteoroid orbits have perihelion distances  $q \lesssim 0.4$  au, that is, within the orbit of Mercury (Table 4). A lack of low- $q$  orbits has also been reported for fireballs produced by meter-scale Earth impacting meteoroids in general (Brown et al., 2016). A similar lack of objects having orbits with  $q < 0.4$  AU is present in the collection of 57 fireballs reported by Halliday et al. (1996) having terminal masses in excess of 100 g and therefore probable meteorite producers. Super-catastrophic disruptions of asteroids at small  $q$  was recently proposed by Granvik et al. (2016) as an explanation for the lack of known NEOs at small  $q$ . As mentioned in Sect. 2.2, the model by Granvik et al. (2016) was calibrated with the observed distribution of NEOs with  $17 < H < 25$ , that is, diameters  $35 \text{ m} \lesssim D \lesssim 1.4 \text{ km}$  when assuming a geometric albedo  $p_V = 0.14$ . As shown in the same paper there is a linear correlation between  $H$  and the perihelion distance at which

Table 1: Equivalent trajectory data for meteorite falls having instrumentally measured orbits. All angular elements are J2000.0. Latitude and longitude for the reference positions, equivalent equatorial geocentric radiant coordinates, speeds prior to deceleration from the Earth's atmosphere ( $v_\infty$ ) are extracted from references, but modified to agree with published primary data in some cases. In cases where references do not provide formal errors, the last significant figure is taken as the uncertainty.

Meteorite name	Fall date and time		Lat [deg]	Lon [deg]	RA [deg]	Dec [deg]	$v_{\infty}$ [km/s]	Ref.
	UTC							
Příbram	1959-04-07	19.5033	49.510	14.830	192.34 ± 0.01	17.47 ± 0.01	20.93 ± 0.01	27,34,35
Lost City	1970-01-04	2.2333	36.005	-95.090	315.0 ± 0.1	39.0 ± 0.1	14.235 ± 0.002	18,19,20
Innisfree	1977-02-06	2.2939	53.415	-111.338	7.43 ± 0.3	66.52 ± 0.01	14.5 ± 0.1	13,14
Benešov	1991-05-07	23.0647	49.662	14.635	227.62 ± 0.01	39.909 ± 0.002	21.272 ± 0.005	4,5
Peekskill	1992-10-09	23.8000	39.663	-78.206	208.9 ± 0.2	-29.2 ± 0.3	14.72 ± 0.050	27,32,33
Tagish Lake	2000-01-18	16.7283	60.000	-134.200	90.4 ± 1.9	29.9 ± 2.8	15.8 ± 0.6	38,39,40
Morávka	2000-05-06	11.8639	50.230	18.450	250.1 ± 0.7	54.95 ± 0.25	22.5 ± 0.3	26,27
Neuschwanstein	2002-04-06	20.3383	47.304	11.552	192.33 ± 0.03	19.55 ± 0.04	20.960 ± 0.040	28,29
Park Forest	2003-03-27	5.8406	41.130	-87.900	171.8 ± 1.3	11.2 ± 0.5	19.5 ± 0.3	31
Villalbeto de la Peña	2004-01-04	16.7792	42.771	-4.789	311.4 ± 1.4	-18.0 ± 0.7	16.90 ± 0.40	41,42
Bunburra Rockhole	2007-07-20	19.2311	-31.450	129.827	80.70 ± 0.05	-14.22 ± 0.04	13.395 ± 0.007	6
Almahata Sitta	2008-10-07	2.7611	20.858	31.804	348.1 ± 0.1	7.6 ± 0.1	12.760 ± 0.001	1,2
Buzzard Coulee	2008-11-21	0.4453	53.183	-109.875	290.0 ± 0.7	77.0 ± 0.3	18.05 ± 0.40	7,8
Maribo	2009-01-17	19.1411	54.585	13.657	124.7 ± 1.0	19.7 ± 0.5	28.30 ± 0.20	21,22,23,24
Jesenice	2009-04-09	0.9944	46.662	13.692	159.9 ± 1.2	58.7 ± 0.5	13.80 ± 0.25	15
Grimsby	2009-09-26	1.0496	43.534	-80.194	242.60 ± 0.26	54.98 ± 0.12	20.95 ± 0.19	12
Košice	2010-02-28	22.4128	20.705	48.667	114.3 ± 1.7	29.0 ± 3.0	14.90 ± 0.35	16
Mason Gully	2010-04-13	10.6036	-30.275	128.215	148.36 ± 0.05	9.00 ± 0.05	14.68 ± 0.011	25
Križevci	2011-02-04	23.3444	45.733	16.430	131.22 ± 0.05	19.53 ± 0.04	18.21 ± 0.07	17
Sutter's Mill	2012-04-22	14.6036	38.804	-120.908	24.0 ± 1.3	12.7 ± 1.7	28.6 ± 0.6	36,37
Novato	2012-10-18	2.7417	36.295	-123.463	268.1 ± 0.5	-48.9 ± 0.6	13.75 ± 0.12	30
Chelyabinsk	2013-02-15	3.3389	54.454	64.477	332.81 ± 0.14	0.29 ± 0.14	19.03 ± 0.13	9,10
Annama	2014-04-18	22.2358	68.775	30.787	213.0 ± 0.2	8.8 ± 0.4	24.20 ± 0.50	3
Žd'ár nad Sázavou	2014-12-09	16.2806	49.941	18.002	69.31 ± 0.02	26.98 ± 0.02	21.97 ± 0.030	43
Ejby	2016-02-06	21.0750	55.449	11.912	77.74 ± 0.09	26.89 ± 0.38	14.50 ± 0.100	11

<sup>1</sup>Jenniskens et al. (2009) <sup>2</sup>Welten et al. (2010) <sup>3</sup>Trigo-Rodríguez et al. (2015) <sup>4</sup>Spurný (1994) <sup>5</sup>Borovička et al. (1998) <sup>6</sup>Spurný et al. (2012a) <sup>7</sup>Milley et al. (2010) <sup>8</sup>Milley (2010) <sup>9</sup>Borovička et al. (2013a) <sup>10</sup>Brown et al. (2013) <sup>11</sup>Spurný et al. (2016a) <sup>12</sup>Brown et al. (2011) <sup>13</sup>Halliday et al. (1978) <sup>14</sup>Halliday et al. (1981) <sup>15</sup>Spurný et al. (2010) <sup>16</sup>Borovička et al. (2013b) <sup>17</sup>Borovička et al. (2015b) <sup>18</sup>McCrosky et al. (1971) <sup>19</sup>Cepplecha (1996) <sup>20</sup>Cepplecha and ReVelle (2005) <sup>21</sup>Kener D and G (2009) <sup>22</sup>Haak et al. (2010) <sup>23</sup>Haak et al. (2011) <sup>24</sup>Spurný et al. (2013) <sup>25</sup>Spurný et al. (2012b) <sup>26</sup>Borovička et al. (2003) <sup>27</sup>Borovička and Kalenda (2003) <sup>28</sup>Spurný et al. (2003) <sup>29</sup>Spurný et al. (2002) <sup>30</sup>Jenniskens et al. (2014) <sup>31</sup>Brown et al. (2004) <sup>32</sup>Brown et al. (1994) <sup>33</sup>Cepplecha et al. (1996) <sup>34</sup>Cepplecha (1961) <sup>35</sup>Cepplecha (1977) <sup>36</sup>Jenniskens et al. (2012) <sup>37</sup>Nishiizumi et al. (2014) <sup>38</sup>Brown et al. (2001) <sup>39</sup>Hildebrand et al. (2006) <sup>40</sup>Brown et al. (2002) <sup>41</sup>Trigo-Rodríguez et al. (2006) <sup>42</sup>Llorca et al. (2005) <sup>43</sup>Spurný (2015)

Table 2: Geophysical data for meteorite falls having instrumentally measured orbits. This includes meteorite classification, bulk density and cosmic-ray exposure age (CRE). All data are extracted from the associated references.

Meteorite name	Classification	Ref.	Bulk density [kg m <sup>-3</sup> ]	Ref.	CRE age [Myr]	Ref.
Příbram	H5	<sup>73</sup>	3570	<sup>46</sup>	12	<sup>47</sup>
Lost City	H5	<sup>74</sup>	—		8	<sup>48</sup>
Innisfree	L5/LL5(?)	<sup>75</sup>	—		26–28	<sup>49</sup>
Benešov	H5/LL3.5	<sup>76</sup>	—		—	
Peekskill	H6	<sup>77</sup>	—		32	<sup>50</sup>
Tagish Lake	C2	<sup>40</sup>	1640	<sup>41</sup>	>3	<sup>51</sup>
Morávka	H5	<sup>28</sup>	3590	<sup>28</sup>	5.7–7.7	<sup>28</sup>
Neuschwanstein	EL6	<sup>52</sup>	3500	<sup>53</sup>	43–51	<sup>52</sup>
Park Forest	L5	<sup>33</sup>	3370	<sup>54</sup>	12–16	<sup>55</sup>
Villalbeto de la Peña	L6	<sup>44</sup>	3420	<sup>44</sup>	43–53	<sup>44</sup>
Bunburra Rockhole	Euc-Anom	<sup>56</sup>	—		22	<sup>57</sup>
Almahata Sitta	Ure-Anom	<sup>1</sup>	2900–3300	<sup>58</sup>	16–22	<sup>59</sup>
Buzzard Coulee	H4	<sup>60</sup>	3370–3550	<sup>61</sup>	—	
Maribo	CM2	<sup>62</sup>	—		0.8–1.4	<sup>62</sup>
Jesenice	L6	<sup>63</sup>	—		4	<sup>63</sup>
Grimsby	H5	<sup>64</sup>	3340–3370	<sup>64</sup>	21–26	<sup>13</sup>
Košice	H5	<sup>65</sup>	3320–3540	<sup>66</sup>	5–7	<sup>78</sup>
Mason Gully	H5	<sup>67</sup>	3280–3360	<sup>54</sup>	—	
Križevci	H6	<sup>68</sup>	—		—	
Sutter’s Mill	CM2	<sup>69</sup>	2156–2358	<sup>38</sup>	0.074–0.09	<sup>39</sup>
Novato	L6	<sup>31</sup>	3190–3350	<sup>31</sup>	8–10	<sup>31</sup>
Chelyabinsk	LL5	<sup>70</sup>	3321–3329	<sup>70</sup>	1	<sup>71</sup>
Annama	H5	<sup>72</sup>	3500	<sup>72</sup>	26–34	<sup>72</sup>
Žd’ár nad Sázavou	L3/L3.9	<sup>45</sup>	3050	<sup>45</sup>	—	
Ejby	H5/6	<sup>11</sup>	—		—	

<sup>1</sup>Jenniskens et al. (2009) <sup>11</sup>Spurný et al. (2016a) <sup>13</sup>Cartwright et al. (2010) <sup>28</sup>Borovička and Kalenda (2003) <sup>31</sup>Jenniskens et al. (2014) <sup>33</sup>Simon et al. (2004) <sup>38</sup>Jenniskens et al. (2012) <sup>39</sup>Nishiizumi et al. (2014) <sup>40</sup>Brown et al. (2001) <sup>41</sup>Hildebrand et al. (2006) <sup>44</sup>Llorca et al. (2005) <sup>45</sup>Spurný (2015) <sup>46</sup>Britt and Consolmagno (2003) <sup>47</sup>Stauffer and Urey (1962) <sup>48</sup>Baxter and Funkhouser (1971) <sup>49</sup>Goswami et al. (1978) <sup>50</sup>Graf et al. (1997) <sup>51</sup>Herzog and Caffee (2014) <sup>52</sup>Zipfel et al. (2010) <sup>53</sup>Kohout et al. (2010) <sup>54</sup>Macke (2010) <sup>55</sup>Meier et al. (2017) <sup>56</sup>Bland et al. (2009) <sup>57</sup>Welten et al. (2012) <sup>58</sup>Kohout et al. (2011) <sup>59</sup>Horstmann and Bischoff (2014) <sup>60</sup>Hutson et al. (2009) <sup>61</sup>Fry et al. (2013) <sup>62</sup>Haak et al. (2012) <sup>63</sup>Bischoff et al. (2011) <sup>64</sup>McCausland et al. (2010) <sup>65</sup>Ozdfn et al. (2015) <sup>66</sup>Kohout et al. (2014b) <sup>67</sup>Dyl et al. (2016) <sup>68</sup>Lyon et al. (2014) <sup>69</sup>Zolensky et al. (2014) <sup>70</sup>Kohout et al. (2014a) <sup>71</sup>Richter et al. (2015) <sup>72</sup>Kohout et al. (2016) <sup>73</sup>Tucek (1961) <sup>74</sup>Nava et al. (1971) <sup>75</sup>Kallemeyn et al. (1989) <sup>76</sup>Spurný et al. (2014) <sup>77</sup>Wlotzka (1993) <sup>78</sup>Povinec et al. (2015)

Table 3: Orbital elements for meteorite-dropping fireballs. Semimajor axis ( $a$ ), eccentricity  $e$ , inclination  $i$ , longitude of ascending node  $\Omega$ , argument of perihelion  $\omega$ .

Meteorite name	$a$ [au]	$e$	$i$ [deg]	$\Omega$ [deg]	$\omega$ [deg]	MJD UTC
Příbram	$2.4050 \pm 0.0043$	$0.6717 \pm 0.0006$	$10.4841 \pm 0.0086$	$17.8019 \pm 0.0000$	$241.723 \pm 0.020$	36665.812639
Lost City	$1.6486 \pm 0.0037$	$0.4133 \pm 0.0013$	$11.940 \pm 0.025$	$283.7568 \pm 0.0000$	$160.67 \pm 0.14$	40590.093056
Imisfree	$1.866 \pm 0.051$	$0.472 \pm 0.014$	$12.250 \pm 0.22$	$317.5223 \pm 0.0002$	$177.97 \pm 0.13$	43180.095579
Benešov	$2.4826 \pm 0.0024$	$0.6273 \pm 0.0004$	$23.9807 \pm 0.0074$	$47.0004 \pm 0.0000$	$218.369 \pm 0.017$	48383.961030
Peekskill	$1.489 \pm 0.015$	$0.4052 \pm 0.0055$	$4.88 \pm 0.15$	$17.0289 \pm 0.0001$	$307.46 \pm 0.61$	48904.991667
Tagish Lake	$1.98 \pm 0.19$	$0.554 \pm 0.045$	$2.06 \pm 0.97$	$297.9013 \pm 0.0007$	$224.3 \pm 2.5$	51561.697014
Morávka	$1.851 \pm 0.079$	$0.469 \pm 0.022$	$32.28 \pm 0.42$	$46.2573 \pm 0.0000$	$203.5 \pm 1.8$	51670.494329
Neuschwanstein	$2.398 \pm 0.017$	$0.6693 \pm 0.0024$	$11.416 \pm 0.032$	$16.8257 \pm 0.0000$	$241.185 \pm 0.061$	52370.847431
Park Forest	$2.53 \pm 0.21$	$0.680 \pm 0.025$	$3.25 \pm 0.66$	$6.1153 \pm 0.0003$	$237.5 \pm 2.0$	52725.243356
Villalbeto de la Peña	$2.30 \pm 0.22$	$0.627 \pm 0.036$	$0.02 \pm 0.49$	$282 \pm 180$	$134 \pm 180$	53008.699132
Bumburra Rockhole	$0.8530 \pm 0.0010$	$0.2425 \pm 0.0014$	$8.937 \pm 0.072$	$297.5945 \pm 0.0000$	$210.04 \pm 0.15$	54301.801296
Almahata Sitta	$1.3085 \pm 0.0003$	$0.3060 \pm 0.0001$	$2.4373 \pm 0.0023$	$194.0822 \pm 0.0000$	$232.405 \pm 0.019$	54746.115046
Buzzard Coulee	$1.246 \pm 0.029$	$0.228 \pm 0.018$	$25.07 \pm 0.78$	$238.9374 \pm 0.0001$	$211.3 \pm 1.5$	54791.018553
Maribo	$2.48 \pm 0.27$	$0.807 \pm 0.015$	$0.1 \pm 1.3$	$297 \pm 48$	$279 \pm 49$	54848.797546
Jesenice	$1.744 \pm 0.068$	$0.429 \pm 0.023$	$9.58 \pm 0.48$	$19.1950 \pm 0.0002$	$190.49 \pm 0.54$	54930.041435
Grimstby	$2.035 \pm 0.048$	$0.518 \pm 0.011$	$28.08 \pm 0.28$	$182.9560 \pm 0.0000$	$159.85 \pm 0.24$	55100.043731
Košice	$2.73 \pm 0.23$	$0.650 \pm 0.030$	$1.99 \pm 0.47$	$340.0713 \pm 0.0024$	$204.2 \pm 1.5$	55255.933866
Mason Gully	$2.5566 \pm 0.0094$	$0.6159 \pm 0.0014$	$0.895 \pm 0.032$	$203.2134 \pm 0.0015$	$19.01 \pm 0.08$	55299.441817
Křiževci	$1.5428 \pm 0.0087$	$0.5205 \pm 0.0034$	$0.638 \pm 0.026$	$315.5544 \pm 0.0035$	$254.383 \pm 0.081$	55596.972685
Sutter's Mill	$2.57 \pm 0.38$	$0.823 \pm 0.022$	$2.4 \pm 1.5$	$32.716 \pm 0.015$	$77.9 \pm 3.3$	56039.608484
Novato	$2.091 \pm 0.079$	$0.528 \pm 0.018$	$5.52 \pm 0.11$	$24.9625 \pm 0.0002$	$347.36 \pm 0.30$	56218.114236
Chelyabinsk	$1.770 \pm 0.022$	$0.5792 \pm 0.0061$	$4.78 \pm 0.13$	$326.4136 \pm 0.0003$	$109.22 \pm 0.18$	56338.139120
Annama	$2.08 \pm 0.13$	$0.690 \pm 0.021$	$14.23 \pm 0.49$	$28.5990 \pm 0.0001$	$263.08 \pm 0.74$	56765.926493
Žďár nad Sázavou	$2.1020 \pm 0.0088$	$0.6808 \pm 0.0015$	$2.809 \pm 0.018$	$257.2618 \pm 0.0002$	$257.748 \pm 0.043$	57000.678356
Ejby	$2.805 \pm 0.094$	$0.655 \pm 0.012$	$0.958 \pm 0.098$	$317.2078 \pm 0.0080$	$197.75 \pm 0.25$	57424.878125

the disruption typically happens,  $q^*$ . A simple linear extrapolation in  $(H, q^*)$  space from the model's lower diameter limit of about  $D \approx 35$  m down to  $D \approx 1$  m ( $H \approx 32$ ) suggests that for 1-meter-diameter objects  $q^* \approx 0.38$  au. This is remarkably well in agreement with the fireball data and suggest that the lack of meter-scale meteoroids with  $q \lesssim 0.4$  au is real and that, similar to larger asteroids, they are destroyed at non-trivial distances from the Sun. In addition, whatever mechanism or mechanisms are destroying these objects, the correlation between disruption distance and size is remarkably simple over a size range covering more than three orders of magnitude.

The aphelion distances are all well within the perihelion distance of Jupiter indicating that these objects are detached from Jupiter's direct influence. This suggests that they are of asteroidal rather than cometary origin. The only border-line cases are those with  $Q \gtrsim 4.5$  au, that is, Košice, Ejby, Maribo, and Sutter's Mill. Especially for the latter two the probability for a cometary origin is increased because of their classification as carbonaceous chondrites. The strong anticorrelation between strong, probable meteorite-producing fireballs, and trans-Jovian orbits is apparent in the larger set of Prairie Network (PN) fireball data as well (Wetherill and ReVelle, 1982), indicating that very few obviously cometary fireballs yield meteorites.

#### 4.2. Escape routes and source regions

Based on the orbits derived above we first estimate the likely ERs for these meteorites. Table 5 provides estimates of each meteorite-producing fireball's probable ER based on its measured orbit using a debiased low-resolution model for NEO ERs (see Sect. 2.2). The differences are negligible when using an 8 times higher resolution for the orbital distribution as shown in Table 6. The insensitivity to the resolution of the orbital distribution suggests that even the low resolution is able to reproduce the typical dynamical features in the steady-state orbit distributions for each ER. It thus implies that estimates of the most likely ERs will not become more accurate by increasing the resolution of the orbit model (see discussion in Sect. 4.3).

When correlating meteorite types with their likely ERs it becomes clear that the inner main belt and the Hungaria group are the likely ERs for almost all known meteorite falls (Fig. 1). However, for meteorites (or their parent bodies) escaping the main belt through the 3:1J MMR, we cannot rule out an origin in the middle belt combined with subsequent orbital evolution to a smaller semimajor axis, such as through Yarkovsky drift. There is, nevertheless, substantial evidence from current meteorite orbits and the present delivery model that few meteorite falls directly originate in the outer main belt or from the immediate JFC population. The bias is largely explained by orbital dynamics as asteroids from the outer main belt have a small contribution to the part of NEO orbital-element phase space that harbor the most likely Earth-impacting orbits, that is, those with  $a \sim 1$  au,  $e \sim 0$ , and  $i \sim 0^\circ$ .

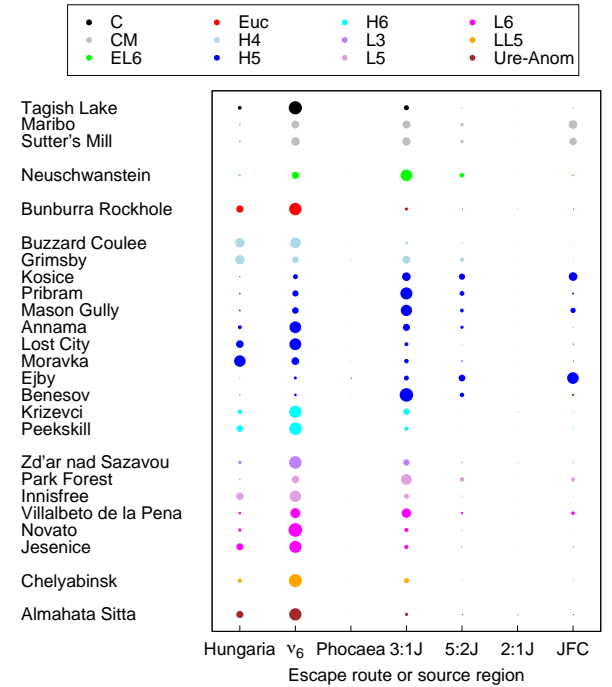


Figure 1: Escape regions for different meteorite groups. The area of the filled circle is proportional to the probability that the meteorite originates in that source region or escapes the main asteroid belt through that escape route. Note that Benešov and Innisfree have mixed classifications as shown in Table 2 of LL3 and LL5, respectively.

The material strength of meteoroids can be expected to also cause (a part of) this bias, particularly assuming outer belt asteroids and JFCs are composed of weaker material which is much more easily destroyed upon impact with the Earth's atmosphere leaving no macroscopic meteorites to be found. This notion is consistent with the fireball record (Flynn et al., 2017) where most fireballs having comet-like orbits also have lower penetrating ability on average, indicative of more fragile structure, than fireballs on more asteroid-like orbits, a long established result (Wetherill and ReVelle, 1982; Borovička, 2007).

Asteroid types with weaker material strength are also expected to be fairly common in the inner belt in the size range of meteorite parent bodies (DeMeo and Carry, 2014). While there are 3 carbonaceous chondrites among the known meteorite producing falls with orbits, this still amounts to only about 13% of the entire sample, almost an order of magnitude higher than the relative abundance of carbonaceous chondrites among all recovered meteorites (3.5%).

In contrast, approximately 1/3 of asteroids with diameters  $5 \text{ km} < D < 20 \text{ km}$  in the inner main-belt are C types, while the fraction of NEOs which are C-types is in the 20-35% range (Binzel et al., 2015). It is notable, that these three meteorite producing fireballs are also extraordinary in that they were all produced by comparatively large impactors, ranging from 1.5 tonnes for Maribo to 56

Table 4: Orbital parameters for meteorite-dropping fireballs computed from their apparent radiant. The epoch of osculation for  $q$  and  $Q$  is identical to that in Table 3. Here  $v_g$  is the geocentric speed of the meteoroid prior to impact, that is, the speed it would have in the absence of gravitational acceleration, whereas  $v_h$  is the heliocentric velocity of the meteorite at the epoch of impact.

Meteorite name	$q$ [au]	$Q$ [au]	$v_g$ [km/s]	$v_h$ [km/s]
Příbram	$0.7896 \pm 0.0001$	$4.0204 \pm 0.0087$	$17.437 \pm 0.012$	$37.4600 \pm 0.0089$
Lost City	$0.9672 \pm 0.0002$	$2.3300 \pm 0.0074$	$9.1984 \pm 0.0018$	$35.584 \pm 0.017$
Innisfree	$0.9860 \pm 0.0000$	$2.75 \pm 0.10$	$9.40 \pm 0.23$	$36.38 \pm 0.18$
Benešov	$0.9252 \pm 0.0001$	$4.0401 \pm 0.0048$	$18.0807 \pm 0.0059$	$37.4271 \pm 0.0046$
Peekskill	$0.8856 \pm 0.0018$	$2.093 \pm 0.029$	$10.090 \pm 0.075$	$34.369 \pm 0.087$
Tagish Lake	$0.884 \pm 0.011$	$3.08 \pm 0.39$	$11.31 \pm 0.84$	$36.82 \pm 0.59$
Morávka	$0.9822 \pm 0.0038$	$2.72 \pm 0.16$	$19.60 \pm 0.23$	$35.77 \pm 0.28$
Neuschwanstein	$0.7930 \pm 0.0004$	$4.003 \pm 0.033$	$17.506 \pm 0.048$	$37.453 \pm 0.034$
Park Forest	$0.8107 \pm 0.0098$	$4.251 \pm 0.419$	$16.05 \pm 0.37$	$37.79 \pm 0.39$
Villalbeto de la Peña	$0.8596 \pm 0.0074$	$3.75 \pm 0.45$	$12.92 \pm 0.53$	$37.67 \pm 0.50$
Bunburra Rockhole	$0.6461 \pm 0.0019$	$1.0599 \pm 0.0003$	$6.735 \pm 0.039$	$26.571 \pm 0.022$
Almahata Sitta	$0.9081 \pm 0.0000$	$1.7088 \pm 0.0005$	$6.8024 \pm 0.0019$	$33.1258 \pm 0.0021$
Buzzard Coulee	$0.9612 \pm 0.0015$	$1.530 \pm 0.058$	$14.19 \pm 0.51$	$32.92 \pm 0.25$
Maribo	$0.478 \pm 0.018$	$4.48 \pm 0.52$	$25.80 \pm 0.22$	$38.03 \pm 0.51$
Jesenice	$0.9965 \pm 0.0007$	$2.49 \pm 0.14$	$8.28 \pm 0.42$	$35.54 \pm 0.28$
Grimsby	$0.9817 \pm 0.0003$	$3.088 \pm 0.096$	$17.89 \pm 0.22$	$36.52 \pm 0.14$
Košice	$0.9563 \pm 0.0042$	$4.50 \pm 0.47$	$10.31 \pm 0.44$	$38.29 \pm 0.36$
Mason Gully	$0.9820 \pm 0.0002$	$4.131 \pm 0.019$	$9.324 \pm 0.016$	$37.715 \pm 0.017$
Križevci	$0.7397 \pm 0.0012$	$2.346 \pm 0.019$	$14.456 \pm 0.089$	$34.995 \pm 0.047$
Sutter's Mill	$0.456 \pm 0.022$	$4.69 \pm 0.74$	$25.96 \pm 0.65$	$37.68 \pm 0.67$
Novato	$0.9879 \pm 0.0004$	$3.19 \pm 0.16$	$8.22 \pm 0.20$	$36.83 \pm 0.22$
Chelyabinsk	$0.7447 \pm 0.0021$	$2.795 \pm 0.045$	$15.14 \pm 0.16$	$35.99 \pm 0.086$
Annama	$0.6436 \pm 0.0054$	$3.51 \pm 0.26$	$21.45 \pm 0.56$	$36.60 \pm 0.36$
Ždár nad Sázavou	$0.6709 \pm 0.0003$	$3.533 \pm 0.018$	$18.607 \pm 0.035$	$37.141 \pm 0.024$
Ejby	$0.9677 \pm 0.0006$	$4.64 \pm 0.19$	$9.44 \pm 0.15$	$38.51 \pm 0.14$



Table 5: Probabilities of different escape regions for meteorite falls based on the low-resolution NEO orbit model. Meteorite classification has been included to help interpretation.

Meteorite name	Classification	Hungaria [%]	$\nu_6$ [%]	Phocaea [%]	3:1J [%]	5:2J [%]	2:1J [%]	JFC [%]
Příbram	H5	$0.8 \pm 0.4$	$15 \pm 7$	$0.0 \pm 0.3$	$70 \pm 20$	$10 \pm 9$	$0.0 \pm 0.2$	$2 \pm 2$
Lost City	H5	$24 \pm 7$	$69 \pm 8$	$0.0 \pm 0.2$	$7 \pm 2$	$0.3 \pm 0.2$	$0.02 \pm 0.06$	$0 \pm 0$
Innisfree	L5/LL5?	$28 \pm 4$	$60 \pm 4$	$0.0 \pm 0.5$	$11 \pm 2$	$1.1 \pm 0.5$	$0.0 \pm 0.1$	$0 \pm 0$
Benešov	H5/LL3.5	$0.8 \pm 0.4$	$5 \pm 2$	$0 \pm 7$	$80 \pm 30$	$9 \pm 9$	$0.1 \pm 0.3$	$2 \pm 3$
Peekskill	H6	$20 \pm 3$	$72 \pm 4$	$0.00 \pm 0.07$	$7 \pm 1$	$0.17 \pm 0.08$	$0.0 \pm 0.1$	$0 \pm 0$
Tagish Lake	C2	$6.7 \pm 0.6$	$82 \pm 2$	$0.00 \pm 0.01$	$11 \pm 1$	$0.28 \pm 0.09$	$0.004 \pm 0.006$	$0.2 \pm 0.1$
Morávka	H5	$61 \pm 5$	$27 \pm 3$	$0 \pm 2$	$10 \pm 1$	$1.2 \pm 0.4$	$0.04 \pm 0.05$	$0 \pm 0$
Neuschwanstein	EL6	$1.4 \pm 0.4$	$26 \pm 6$	$0.0 \pm 0.2$	$63 \pm 13$	$9 \pm 6$	$0.0 \pm 0.1$	$1 \pm 1$
Park Forest	L5	$1.6 \pm 0.2$	$25 \pm 3$	$0.001 \pm 0.006$	$48 \pm 5$	$11 \pm 4$	$0.1 \pm 0.1$	$15 \pm 5$
Villalbeto de la Peña	L6	$3.4 \pm 0.3$	$50 \pm 2$	$0.001 \pm 0.006$	$41 \pm 3$	$2.7 \pm 0.8$	$0.03 \pm 0.04$	$3 \pm 1$
Bunburra Rockhole	Euc- Anom	$24 \pm 7$	$68 \pm 9$	$0.00 \pm 0.04$	$7 \pm 3$	$0 \pm 0$	$0.1 \pm 0.5$	$0 \pm 0$
Almahata Sitta	Ure - Anom	$25 \pm 7$	$70 \pm 9$	$0.0 \pm 0.2$	$5 \pm 2$	$0 \pm 0$	$0 \pm 1$	$0 \pm 0$
Buzzard Coulee	H4	$38 \pm 7$	$55 \pm 7$	$0.0 \pm 0.7$	$5 \pm 1$	$2 \pm 2$	$0 \pm 0$	$0 \pm 0$
Maribo	CM2	$2.3 \pm 0.3$	$33 \pm 3$	$0.000 \pm 0.006$	$36 \pm 4$	$6 \pm 2$	$0.07 \pm 0.09$	$22 \pm 8$
Jesenice	L6	$21 \pm 31$	$70 \pm 3$	$0.00 \pm 0.06$	$9 \pm 1$	$0.5 \pm 0.2$	$0.01 \pm 0.03$	$0 \pm 0$
Grimsbj	H5	$45 \pm 6$	$23 \pm 3$	$0 \pm 5$	$25 \pm 4$	$7 \pm 2$	$0.1 \pm 0.1$	$0.0010 \pm 0.0008$
Košice	H5	$0.7 \pm 0.1$	$13 \pm 2$	$0.000 \pm 0.003$	$37 \pm 4$	$16 \pm 5$	$0.08 \pm 0.09$	$33 \pm 11$
Mason Gully	H5	$1.1 \pm 0.5$	$21 \pm 8$	$0 \pm 0$	$64 \pm 18$	$7 \pm 7$	$0.0 \pm 0.2$	$7 \pm 9$
Křiževci	H6	$10 \pm 2$	$73 \pm 6$	$0.00 \pm 0.05$	$17 \pm 4$	$0.6 \pm 0.4$	$0 \pm 0$	$0 \pm 0$
Sutter's Mill	CM2	$2.6 \pm 0.3$	$36 \pm 3$	$0.001 \pm 0.006$	$31 \pm 3$	$5 \pm 1$	$0.07 \pm 0.08$	$26 \pm 11$
Novato	L6	$4.6 \pm 0.9$	$89 \pm 5$	$0.000 \pm 0.006$	$6 \pm 1$	$0.3 \pm 0.2$	$0.0004 \pm 0.0006$	$0.08 \pm 0.08$
Chelyabinsk	LL5	$8 \pm 3$	$80 \pm 8$	$0.0 \pm 0.1$	$11 \pm 4$	$0.7 \pm 0.7$	$0.01 \pm 0.02$	$0 \pm 0$
Annama	H5	$6.8 \pm 0.9$	$62 \pm 3$	$0.0 \pm 0.3$	$25 \pm 3$	$5 \pm 2$	$0.04 \pm 0.07$	$0.3 \pm 0.2$
Žd'ár nad Sázavou	L3/L3.9	$6 \pm 1$	$72 \pm 5$	$0.00 \pm 0.02$	$19 \pm 3$	$1.0 \pm 0.5$	$0.002 \pm 0.007$	$1 \pm 1$
Ejby	H5/6	$0.3 \pm 0.1$	$5 \pm 2$	$0 \pm 0$	$15 \pm 7$	$32 \pm 24$	$0.1 \pm 0.3$	$50 \pm 30$

Table 6: Probabilities of different escape regions for meteorite falls based on the high-resolution NEO orbit model. Meteorite classification has been included to help interpretation.

Meteorite name	Classification	Hungaria [%]	$\mu_6$ [%]	Phocaea [%]	3:1J [%]	5:2J [%]	2:1J [%]	JFC [%]
Příbram	H5	$1.0 \pm 0.5$	$18 \pm 8$	$0.0 \pm 0.3$	$70 \pm 20$	$10 \pm 10$	$0.0 \pm 0.2$	$2 \pm 3$
Lost City	H5	$27 \pm 5$	$65 \pm 6$	$0.0 \pm 0.1$	$7 \pm 2$	$0.1 \pm 0.1$	$0.01 \pm 0.04$	$0 \pm 0$
Imnistrée	L5/LI.5?	$26 \pm 2$	$61 \pm 3$	$0.0 \pm 0.2$	$12 \pm 1$	$0.9 \pm 0.3$	$0.03 \pm 0.05$	$0 \pm 0$
Benešov	H5/LI.3.5	$0.5 \pm 0.3$	$3 \pm 2$	$0 \pm 6$	$90 \pm 30$	$9 \pm 9$	$0.1 \pm 0.3$	$2 \pm 3$
Peekskill	H6	$20 \pm 3$	$72 \pm 4$	$0.00 \pm 0.06$	$8 \pm 1$	$0.2 \pm 0.1$	$0.02 \pm 0.06$	$0 \pm 0$
Tagish Lake	C2	$6.7 \pm 0.3$	$81 \pm 1$	$0.001 \pm 0.005$	$11.7 \pm 0.5$	$0.28 \pm 0.04$	$0.004 \pm 0.005$	$0.22 \pm 0.06$
Morávka	H5	$62 \pm 3$	$28 \pm 2$	$0 \pm 1$	$9.5 \pm 0.9$	$0.9 \pm 0.2$	$0.03 \pm 0.03$	$0 \pm 0$
Neuschwanstein	EL6	$1.4 \pm 0.4$	$24 \pm 6$	$0.0 \pm 0.2$	$60 \pm 10$	$10 \pm 7$	$0.0 \pm 0.1$	$1 \pm 2$
Park Forest	L5	$1.6 \pm 0.1$	$27 \pm 2$	$0.001 \pm 0.004$	$53 \pm 3$	$9 \pm 2$	$0.08 \pm 0.06$	$9 \pm 2$
Villalbeto de la Peña	L6	$3.4 \pm 0.2$	$46 \pm 1$	$0.001 \pm 0.004$	$42 \pm 2$	$2.6 \pm 0.4$	$0.05 \pm 0.04$	$6 \pm 1$
Bunburra Rockhole	Euc - Anom	$24 \pm 7$	$71 \pm 9$	$0.00 \pm 0.03$	$5 \pm 2$	$0 \pm 0$	$0.2 \pm 0.9$	$0 \pm 0$
Almahata Sitta	Ure - Anom	$24 \pm 7$	$71 \pm 9$	$0.0 \pm 0.3$	$5 \pm 2$	$0 \pm 0$	$0 \pm 2$	$0 \pm 0$
Buzzard Coulee	H4	$41 \pm 4$	$54 \pm 4$	$0.0 \pm 0.4$	$3.8 \pm 0.6$	$1.0 \pm 0.6$	$0 \pm 0$	$0 \pm 0$
Maribo	CM2	$2.2 \pm 0.2$	$29 \pm 2$	$0.000 \pm 0.003$	$29 \pm 3$	$5 \pm 1$	$0.07 \pm 0.06$	$35 \pm 6$
Jesenice	L6	$23 \pm 1$	$68 \pm 2$	$0.00 \pm 0.03$	$8.0 \pm 0.6$	$0.6 \pm 0.1$	$0.01 \pm 0.02$	$0 \pm 0$
Grimsbj	H5	$41 \pm 5$	$20 \pm 2$	$1 \pm 4$	$29 \pm 4$	$9 \pm 3$	$0.1 \pm 0.1$	$0 \pm 0$
Košice	H5	$0.62 \pm 0.04$	$11.5 \pm 0.7$	$0.000 \pm 0.001$	$35 \pm 2$	$18 \pm 3$	$0.09 \pm 0.05$	$35 \pm 5$
Mason Gully	H5	$1.2 \pm 0.4$	$20 \pm 5$	$0.00 \pm 0.01$	$60 \pm 10$	$7 \pm 5$	$0.0 \pm 0.2$	$13 \pm 9$
Křiževci	H6	$9 \pm 2$	$71 \pm 5$	$0.00 \pm 0.02$	$20 \pm 3$	$0.05 \pm 0.05$	$0 \pm 0$	$0 \pm 0$
Sutter's Mill	CM2	$2.4 \pm 0.1$	$34 \pm 1$	$0.001 \pm 0.003$	$32 \pm 2$	$5.4 \pm 0.8$	$0.07 \pm 0.04$	$26 \pm 5$
Novato	L6	$5.1 \pm 0.6$	$87 \pm 3$	$0.000 \pm 0.003$	$7.5 \pm 0.8$	$0.4 \pm 0.1$	$0.0001 \pm 0.0003$	$0.11 \pm 0.06$
Chelyabinsk	LI.5	$8 \pm 1$	$79 \pm 4$	$0.00 \pm 0.05$	$12 \pm 2$	$0.5 \pm 0.2$	$0.0003 \pm 0.0008$	$0 \pm 0$
Annama	H5	$7.0 \pm 0.4$	$64 \pm 1$	$0.0 \pm 0.1$	$24 \pm 1$	$4.9 \pm 0.7$	$0.05 \pm 0.04$	$0.27 \pm 0.07$
Žďár nad Sázavou	L3/L3.9	$6 \pm 1$	$74 \pm 5$	$0.00 \pm 0.02$	$18 \pm 3$	$0.9 \pm 0.4$	$0 \pm 0$	$0.9 \pm 0.7$
Ejby	H5/6	$0.21 \pm 0.06$	$4 \pm 1$	$0 \pm 0$	$11 \pm 4$	$21 \pm 9$	$0.1 \pm 0.1$	$60 \pm 30$

tonnes for Tagish Lake (Borovička et al., 2015a). Taken together, this suggests a material strength bias is present.

The essentially complete lack of falls connected to the Phocaea group and to asteroids escaping the belt through the 2:1 mean-motion resonance with Jupiter can be explained by both dynamical and material-strength arguments. In terms of dynamical arguments these groups have a factor of several smaller impact probabilities with the Earth compared to other asteroidal sources (Granvik et al., 2018), and hence a collision with the Earth is less likely. As for material strength, the outer asteroid belt is well-known to be mass dominated in carbonaceous asteroids that are assumed to produce weak meteoroids (DeMeo and Carry, 2014). Recently a low albedo (and hence likely carbonaceous) asteroid family was found in the Phocaea region, likely dominating the size distribution of Phocaeas at scales akin to meteoroid parent bodies (Novaković et al., 2017).

CM meteorites have been linked to B-type asteroids (de León et al., 2012) and Ch/Cgh-type asteroids (Vernazza et al., 2016). Ch-like asteroids with a  $0.7\text{-}\mu\text{m}$  hydration band are found across the asteroid belt with a minor preference for the middle belt ( $2.5\text{ au} < a < 2.8\text{ au}$ ) (Rivkin, 2012). B-type asteroids (SMASS II) are also found across the belt with a slight preference for the middle belt. C-type asteroids that lack the  $0.7\text{-}\mu\text{m}$  hydration band are expected to typically be found closer to the Sun where temperatures are high enough to drive out volatiles. Our results show that Tagish Lake, an ungrouped C meteorite, is very likely a sample of such a C-type asteroid as it likely originates in the inner part of the main belt and does not show signs of water. This is in contrast to earlier work (Hildebrand et al., 2006) which suggested a comparatively large probability ( $1/4$ ) that Tagish Lake originated directly from the outer part of the main belt.

Sutter’s Mill and Maribo, the two CM2 meteorites in our sample, have very similar orbits and ER source probabilities. Both have relatively high ER affinities with the JFC population but, even within the upper bounds of uncertainty, are more likely to be from the inner to middle main belt. It is most likely these are from middle belt Ch/Cgh-type or B-type asteroids.

The likely source region for Chelyabinsk, an LL5 meteorite, is in the inner main belt with an escape through  $\nu_6$  as has also previously been shown (Popova et al.). There is some controversy over the classification of Innisfree as either an L5 (generally accepted; Rubin, 1990) or LL5 (Smith, 1980). If Innisfree belongs to the LL5 group it implies that we would have two LL5 meteorites with associated orbits and both indicate a likely origin in the inner main belt with an escape through  $\nu_6$ . This could indicate that these meteorites were originally part of a common parent body. The spectral similarity of LL chondrites and (8) Flora as well as the proximity of the Flora family to  $\nu_6$  has been suggested as evidence for Flora being the parent body of LL chondrites (Vernazza et al., 2008; Dunn et al., 2013). A modern re-analysis could reduce

the uncertainty on the classification of Innisfree, but to the best of our knowledge such a re-analysis has not been performed. We note that Stubenberg, which we do not include in our study as the lack of complete published primary trajectory data does not permit us to do an independent computation consistent with other published events, is an LL6 chondrite. The currently published orbital elements (Spurný et al., 2016b) suggest a high ER-likelihood for  $\nu_6$  (70%) and lesser likelihood for 3:1J and Phocaea (23% and 6%, respectively). Interestingly, Stubenberg’s orbit has the largest probability of originating from the Phocaea group among all our examined cases.

H chondrites comprise almost half our total sample. In most cases an ER from either the 3:1J MMR or the  $\nu_6$  is indicated. This is consistent with some of the H-chondrite’s being from in the inner main belt (Trigo-Rodríguez et al., 2015), potentially linked to (6) Hebe (Gaffey and Gilbert, 1998) or smaller parents located in this zone (Binzel et al., 2015). However, two of the H5 chondrites with measured orbits (Ejby and Košice) show comparatively strong probabilities (with large error) as being from JFCs, a surprising result. This may simply reflect the mixing between main belt asteroids and JFCs which occurs near the  $T_j \approx 3$  region as noted by Tancredi (2014).

The five measured L chondrite orbits are strongly associated with ERs in the inner main belt, in particular the  $\nu_6$  and to a lesser degree the 3:1J MMR. These remain small number statistics, but this is somewhat at odds with an origin from the Gefion family (Nesvorný et al., 2009; Jenniskens et al., 2014) in the outer belt which would require an escape predominantly from the 5:2J or, less likely, the 3:1J MMR.

Our predictions for the ERs of Almahata Sitta and Bunburra Rockhole, both primarily  $\nu_6$ , are in agreement with previous studies (Gayon-Markt et al., 2012; Bland et al., 2009).

The CRE age and bulk density are correlated in the sense that low densities are only measured for meteorites with short CRE ages (Fig. 2). In principle, the correlation could be due to either material properties (low-density materials are more fragile and therefore CRE ages are typically short) or dynamical reasons (low-density materials are more common in the outer asteroid belt and dynamical lifetimes for objects originating in the outer belt are shorter than for objects originating in the inner belt). The latter mechanism is likely to be less important, because  $\nu_6$  is the most likely ER for the meteorites with the lowest densities and short CRE ages (Tagish Lake and Sutter’s Mill). The interpretation is currently based on the measurements of only 13 meteorites, but it can be tested by measuring CRE age and/or bulk density for the remaining 12 meteorites.

Additional insight to the origins of meteorites can be obtained by comparing the CRE age to the dynamical age typical for objects originating in a specific ER. A particular question is whether meteorites separated from their parent bodies while still in the asteroid belt or if they separated

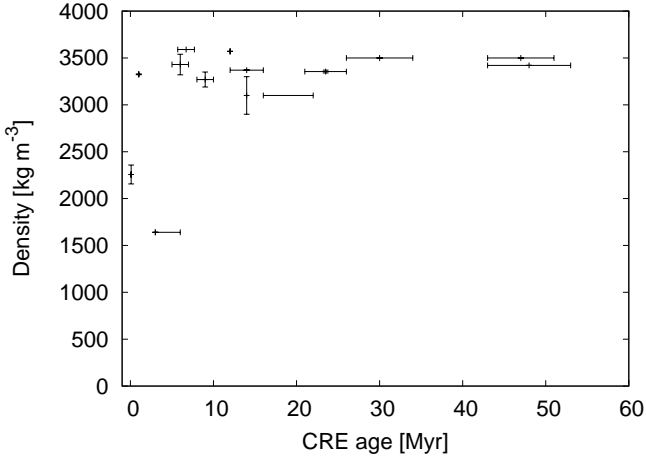


Figure 2: CRE age and bulk density for meteorites for which both have been measured. The error bars show the range of possible values with the nominal value equal to the midpoint of the range. Note that only the nominal value has been reported for many measurements (Table 2). The meteorite with the lowest measured density (Tagish Lake) only has a measured lower limit for the CRE age, but for plotting reasons we have here used an (artificial) upper limit of 6 Myr.

later from NEOs. We estimated the dynamical age of the meteorites by calculating the time it takes for test asteroids in orbital integrations carried out by Granvik et al. (2016) to evolve from a  $q = 1.3$  au orbit to the orbit of the meteorite immediately prior to the impact with the Earth (Table 7). For orbital similarity we required the test asteroid's orbital elements to reproduce the meteorite orbit to within the latter orbit's uncertainty. The relatively small uncertainties implied that only a limited number of test asteroids, out of the more than 90 thousand integrated, ever reached orbits similar to those of the meteorites considered here, and hence the uncertainties are substantial.

By comparing the reported CRE ages to the dynamical ages we find that most meteorites considered here were released from their parent bodies prior to entering their most likely ERs (Fig. 3). This is particularly evident for meteorites with the largest CRE ages. The two apparent outliers that are below the dashed line (Morávka and Grimsby) suffer from small number statistics and the range of dynamical ages cannot be estimated. Hence it is possible that improved statistics in the dynamical analysis would shorten their likely dynamical ages. Given the relatively slow dynamical evolution prior to entering a resonance we find it reasonable to assume that the CRE ages are typically reset at the time of the catastrophic impacts in the main asteroid belt that sends fragments towards planet-crossing orbits. This picture is consistent with the apparent lack of "meteorite-streams" (Pauls and Gladman, 2005) and is further supported by the apparent lack of near-Earth asteroid streams (Schunová et al., 2012). It is broadly consistent with the notion that most of the parent meteoroid's time spent as a meter-sized object is in the main belt undergoing Yarkovsky drift to one of the ERs (Vokrouhlický and Farinella, 2000).

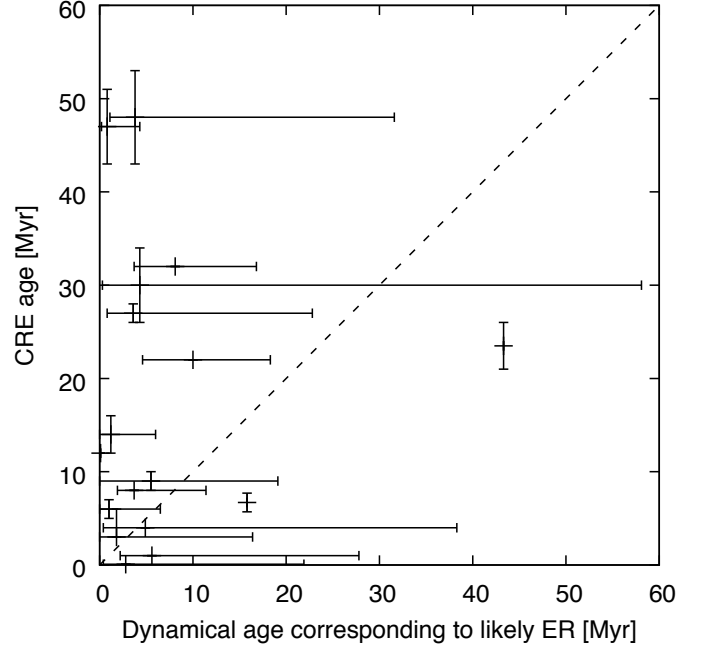


Figure 3: Comparison of dynamical age corresponding to the most likely ER (Table 7) and the reported CRE age (Table 2). The dashed line corresponds to an equal dynamical and CRE age with points above (below) the line implying shorter (longer) dynamical ages than CRE age.

#### 4.3. Sensitivity of ER prediction to accuracy of fireball velocity

In this section we will quantitatively assess the impact that improving the determination of fireball velocity would have on our knowledge of meteorite ERs. We start with the observed atmospheric trajectories for the 25 fireballs discussed above, but rather than using the nominal published values for the velocity uncertainty, we then calculate their heliocentric orbits using 8 different assumptions for the pre-atmosphere velocity uncertainty:  $0.001 \text{ km s}^{-1}$ ,  $0.003 \text{ km s}^{-1}$ ,  $0.01 \text{ km s}^{-1}$ ,  $0.03 \text{ km s}^{-1}$ ,  $0.1 \text{ km s}^{-1}$ ,  $0.3 \text{ km s}^{-1}$ ,  $1 \text{ km s}^{-1}$ , and  $3 \text{ km s}^{-1}$ . Note that the two last velocity uncertainties are larger than reported for any of these events.

As expected, the uncertainty on the orbital elements is reduced when the velocity uncertainty becomes smaller and the radiant uncertainty remains constant (left column in Fig. 4). The apparent insensitivity to velocity uncertainties below about  $0.1 \text{ km s}^{-1}$  is explained as a consequence of a relatively large radiant uncertainty, which is kept at the nominal observed value. At some point the velocity uncertainty becomes negligible compared to the radiant uncertainty which now dominates the total uncertainty budget. An improvement in the orbital uncertainty can thus no longer be obtained by reducing the velocity uncertainty. For example, all but one of the cases that show  $\Delta a > 0.01 \text{ au}$  for a velocity uncertainty of  $0.001 \text{ km s}^{-1}$  have radiant uncertainties  $\geq 0.3^\circ$  whereas the ones that show  $\Delta a < 0.01 \text{ au}$  have radiant uncertainties  $\leq 0.3^\circ$ . The

Table 7: Dynamical age of meteorites assuming an origin in the asteroid belt. The dynamical age is calculated as the time it takes to evolve from an asteroidal ER (at the NEO-MBO border) to the orbit just before impact with the Earth’s atmosphere. We only consider test asteroids whose orbits  $(a, e, i)$  reproduce the meteorite orbits to better than  $1\text{-}\sigma$  as reported in Table 3. The estimates are based on the orbital integration of more than 90 thousand test asteroids as reported by Granvik et al. (2016). The numbers given for each meteorite and ER are median dynamical age in Myr, range of dynamical ages in Myr, and the number of test asteroids that reproduce the meteorite orbit. Dynamical ages corresponding to the most likely ERs are highlighted in boldface font. Note that Maribo and Ejbby are likely to originate from the JFC population. Note also that the orbit of Almahata Sitta is known so accurately that none of the test asteroids available to us reproduce its orbital elements to within the orbital uncertainty.

Meteorite name	Hungaria		$\nu_6$	Phocaea		3:1J	5:2J	2:1J
Příbram	–	–	5.9/0.9–11.0/2	1.5/1.5–1.5/1	–	–	–	–
Lost City	2.3/2.3–2.3/1	–	<b>3.7/1.9–11.4/6</b>	–	–	–	–	–
Innisfree	47.1/47.1–47.1/1	–	<b>3.6/0.8–22.8/7</b>	53.8/53.8–53.8/1	–	16.6/9.5–23.2/5	6.3/1.6–8.3/3	7.1/3.6–10.6/2
Benešov	–	–	–	–	–	<b>0.3/0.3–0.3/1</b>	–	–
Peekskill	60.7/60.7–60.7/1	–	<b>8.1/3.7–16.8/7</b>	167.0/167.0–167.0/1	–	19.1/3.4–24.3/3	–	–
Tagish Lake	74.7/74.7–74.7/1	–	<b>1.8/0.0–16.4/7</b>	115.8/115.8–115.8/1	–	2.3/0.8–7.2/4	11.2/1.6–20.9/2	0.4/0.4–0.4/1
Morávka	<b>15.8/15.8–15.8/1</b>	–	22.4/4.4–167.5/7	79.1/79.1–79.1/1	–	10.1/2.1–17.6/4	8.7/5.0–12.4/2	12.6/12.6–12.6/1
Neuschwanstein	553.7/553.7–553.7/1	–	3.0/0.8–39.5/7	1.0/1.0–1.0/1	–	<b>0.8/0.2–4.3/5</b>	7.6/1.8–13.4/2	–
Park Forest	74.9/74.9–74.9/1	–	7.4/1.4–22.0/7	55.4/55.4–55.4/1	–	<b>1.2/0.0–6.0/5</b>	1.0/0.0–5.8/3	0.6/0.1–0.9/3
Villabeto de la Peña	74.8/74.8–74.8/1	–	<b>3.8/1.1–31.6/7</b>	185.6/185.6–185.6/1	–	0.9/0.0–1.7/4	0.7/0.1–1.5/3	0.1/0.1–0.1/1
Bunburra Rockhole	99.3/99.3–99.3/1	–	<b>10.0/4.6–18.3/3</b>	–	–	–	–	–
Almahata Sitta	–	–	–	–	–	–	–	–
Buzzard Coulee	28.6/28.6–28.6/1	–	<b>13.8/5.8–145.2/7</b>	122.3/122.3–122.3/1	–	26.3/17.8–46.7/3	45.6/21.8–69.3/2	–
Maribo	74.9/74.9–74.9/1	–	3.7/1.8–24.1/7	185.8/185.8–185.8/1	–	1.0/0.0–1.9/4	0.4/0.2–1.0/3	1.5/0.7–6.3/3
Jesenice	296.9/296.9–296.9/1	–	<b>4.9/0.4–38.3/7</b>	53.0/53.0–53.0/1	–	16.6/6.3–24.4/5	11.3/9.5–13.0/2	10.7/10.7–10.7/1
Grimsbý	<b>43.3/43.3–43.3/1</b>	–	56.2/4.0–172.4/7	12.8/12.8–12.8/1	–	3.5/1.6–26.6/5	4.7/2.9–6.6/2	12.4/1.5–23.3/2
Košice	74.9/74.9–74.9/1	–	3.5/0.8–22.6/7	55.5/55.5–55.5/1	–	<b>1.0/0.0–6.5/5</b>	1.0/0.0–5.8/3	0.3/0.2–0.8/3
Mason Gully	0.4/0.4–0.4/1	–	15.4/2.7–20.7/4	–	–	<b>0.2/0.1–3.6/3</b>	–	–
Križevci	1.1/1.1–1.1/1	–	<b>10.4/1.7–18.2/4</b>	–	–	–	–	–
Sutter’s Mill	74.9/74.9–74.9/1	–	<b>2.8/0.4–21.9/7</b>	50.7/50.7–50.7/1	–	0.3/0.0–23.8/5	0.3/0.0–6.2/3	0.4/0.2–1.0/4
Novato	950.3/950.3–950.3/1	–	<b>5.5/0.0–19.1/7</b>	115.8/115.8–115.8/1	–	18.0/0.8–35.2/4	8.0/0.5–15.5/2	–
Chelyabinsk	60.9/60.9–60.9/1	–	<b>5.6/2.2–27.8/7</b>	1.9/1.9–1.9/1	–	2.1/1.3–3.3/3	7.3/1.9–12.6/2	–
Annama	54.9/54.9–54.9/1	–	<b>4.3/0.3–58.1/7</b>	24.3/24.3–24.3/1	–	11.0/0.5–129.5/5	1.3/0.6–1.6/3	8.0/1.7–14.3/2
Zd’nar nad Sazavou	1.0/1.0–1.0/1	–	<b>8.2/2.0–48.9/7</b>	–	–	1.5/0.5–3.4/3	–	–
Ejbby	0.7/0.7–0.7/1	–	21.0/0.7–30.4/7	53.5/53.5–53.5/1	–	0.8/0.4–5.1/4	0.1/0.1–0.3/3	0.3/0.3–0.3/1

only exception to this rule is Příbram which has a radiant uncertainty of only  $0.01^\circ$  and for which a velocity uncertainty of  $0.001 \text{ km s}^{-1}$  results in  $\Delta a \approx 0.013 \text{ au}$ .

Considering the substantial reduction in orbital uncertainty when reducing the velocity uncertainty, it is somewhat surprising that the determination of meteorite ERs—the primary scientific motivation for setting up fireball networks—is much less improved (left column in Figs. 5–8). In all but a few cases the largest improvement takes place when the velocity uncertainty is pushed down to about  $1 \text{ km s}^{-1}$ . It is reassuring to see that in most cases the primary ERs coincide with  $\nu_6$  and 3:1J, the most important NEO ERs. Note also that in all cases the predicted probabilities are substantially different from the prior distribution, i.e., the limiting case in which the observations would provide no constraints on the meteoroid orbit and, further, the ER.

The results change only marginally when the resolution of the NEO model is increased by a factor of 8 (left versus middle column in Figs. 5–8). The explanation for the insensitivity to model resolution is that the model itself is probabilistic. Increasing the model resolution can never result in a unique determination of ER in the volumes of orbital space that harbour most NEOs, because those volumes are fed by multiple ERs. As explained in the Introduction, the physical reason for the non-determinism is the chaotic long-term orbital evolution of NEOs. The chaotic orbital evolution leads to overlapping but statistically distinct steady-state orbit distributions for NEOs originating in different ERs. A comparison of the left and middle columns in Figs. 5–8 suggests that the low-resolution model accurately captures the overall picture and the high-resolution model provides little added value.

The assumption that the radiant uncertainty would not be reduced when the velocity uncertainty is reduced is not entirely correct (Fig. 9). An accurate treatment of the correlation would require detailed consideration of the hardware and trajectory-computation approach for each case; this is not within the scope of this paper, nor is it possible in most cases given the lack of primary published data for each fireball producing meteorite fall.

Instead we take a simplistic approach and assume a linear correlation between the radiant uncertainty and the velocity uncertainty. Based on a linear regression we find that the radiant uncertainty (in degrees) can be approximated as  $3.9\delta v_\infty$  where the constant  $b$  is statistically indistinguishable from zero and hence omitted, and  $\delta v_\infty$  is provided in  $\text{km s}^{-1}$  (Fig. 9). Given the velocity uncertainties used above the radiant uncertainties are approximately  $0.004^\circ$ ,  $0.012^\circ$ ,  $0.04^\circ$ ,  $0.12^\circ$ ,  $0.4^\circ$ ,  $1.2^\circ$ ,  $4^\circ$ ,  $12^\circ$ , respectively. Again, note that the two last radiant uncertainties are larger than reported for any of these events.

In this simple model, the reduced radiant uncertainties that correspond to small velocity uncertainties, lead to orbital uncertainties which are also much reduced (right column in Fig. 4). The reduction of both velocity and radiant uncertainty leads to a corresponding reduction in or-

bit uncertainty, and for most cases there is no indication across the range of uncertainties considered here that the orbital uncertainty would reach a plateau. There are only two events that have clearly different behaviour compared to the rest: Ejby and Sutter’s Mill. The orbital uncertainty for these two reaches a plateau at some hundreds of meters per second.

The ER probabilities estimated with the correlated radiant uncertainties hardly show variation when compared to the ER probabilities estimated using fixed radiant uncertainties, particularly for  $\delta v_\infty \lesssim 0.03 \text{ km s}^{-1}$  (middle versus right column in Figs. 5–8). This is explained by the fact that the more accurate trajectories typically correspond to orbital-element uncertainties smaller than the resolution of the NEO model. Hence an improvement in the orbital accuracy does not directly translate to an improvement in the source probabilities.

To summarize the effect of the correlated radiant and speed uncertainty on the ER prediction uncertainty, we consider the sample average of the maximum range of ER probability (a proxy for the uncertainty) for each ER, and speed and radiant uncertainty value (Fig. 10). The maximum range of ER probabilities for a particular orbit solution is computed by finding the minimum and maximum ER probabilities among the cells in the high-resolution model that are within the orbital-uncertainty volume. The sample averages show a steep reduction in ER-probability uncertainty when reducing the speed uncertainty (and the correlated radiant uncertainty) from  $3 \text{ km/s}$  to about  $0.1$ – $0.3 \text{ km/s}$ . Reducing the speed uncertainty to below  $0.1 \text{ km/s}$  will only have a marginal impact on the uncertainty of the ER probability. We also note that the JFC source will always have an uncertainty greater than 10%.

## 5. Conclusions

In this work, we first computed heliocentric orbits for 25 meteorite falls based on the trajectory information reported in the literature. For several meteorite falls the trajectory information has only been reported in conference abstracts. We urge members of the community to have their trajectory analysis peer-reviewed, and published with enough supporting data to allow colleagues to reproduce their results.

We then used the orbits (including the orbital uncertainties) and the NEO model by Granvik et al. (2016) to estimate the most likely entrance routes (ERs) for the falls. Both for orbits and ERs our results broadly agree with previously published results in that most meteorite falls originate in the inner main asteroid belt and escape through the 3:1J mean-motion resonance or the  $\nu_6$  secular resonance.

We then proceeded to test how the velocity uncertainty affects the results for both orbits and ER probabilities. We found that pushing the velocity uncertainty below some tens of meters per second does not lead to a substantial reduction of uncertainties related to ER probabilities. Sim-

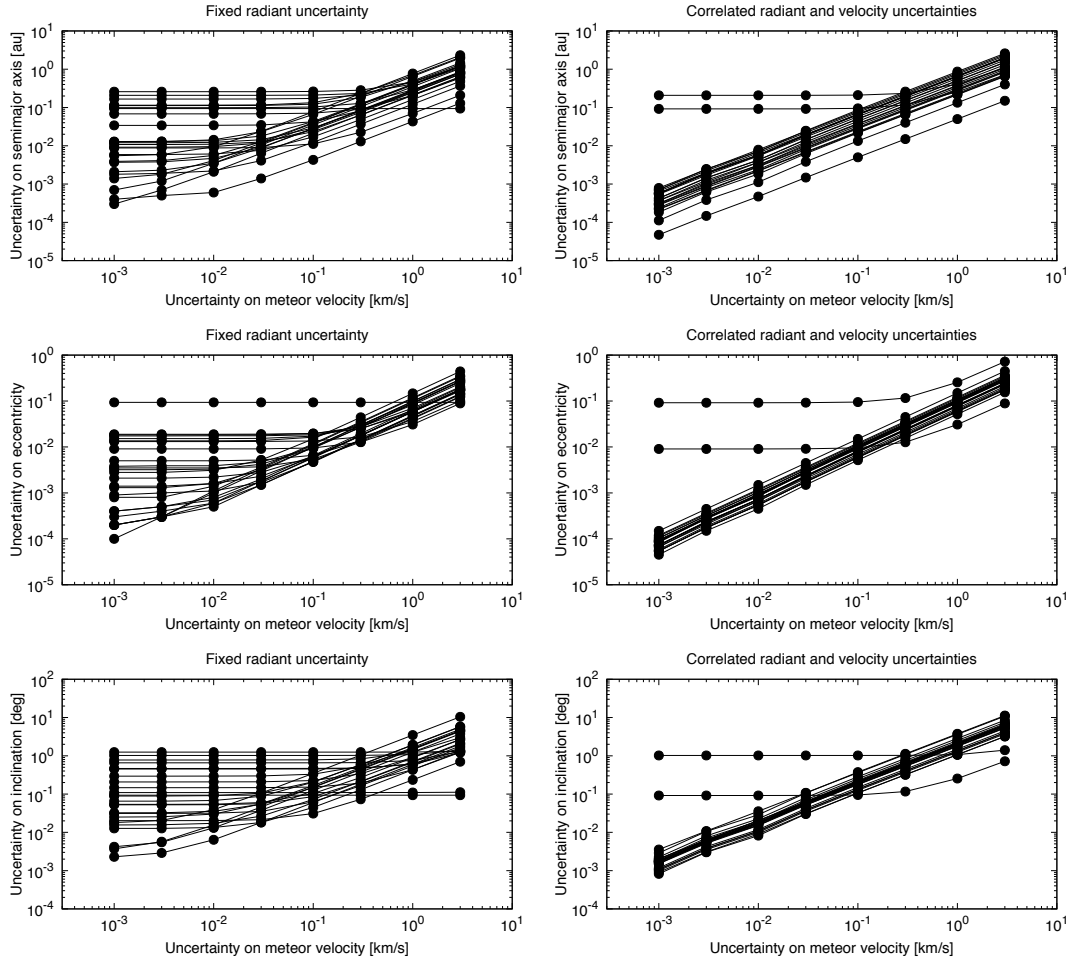


Figure 4: Resulting orbital-element uncertainty as a function of assumed velocity uncertainty when using a fixed radiant uncertainty (left) and a radiant uncertainty correlated with the velocity uncertainty (right).

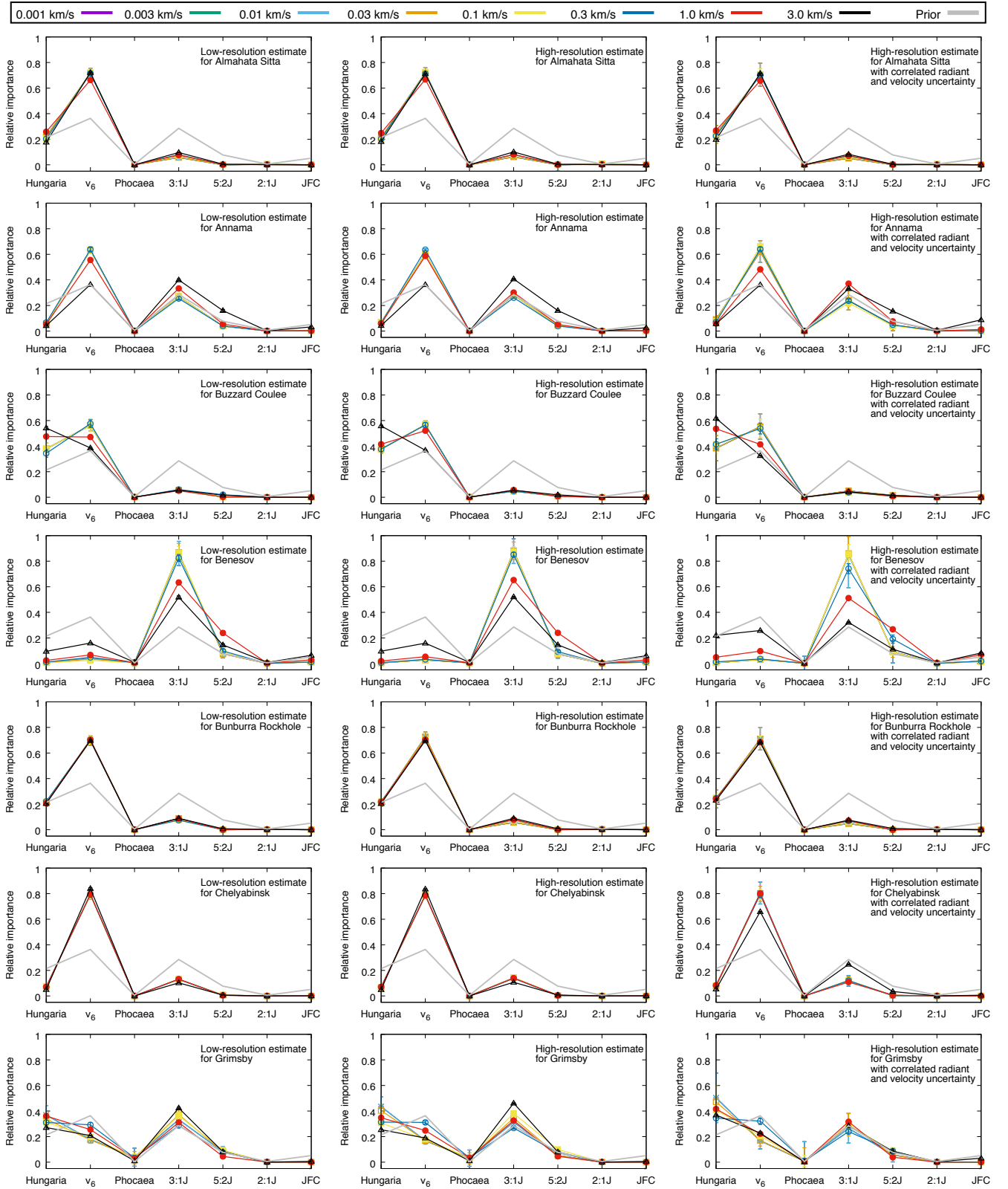


Figure 5: ER prediction corresponding to different speed uncertainties (defined in the legend) based on low-resolution model with fixed radiant uncertainty for the meteor (left), high-resolution model with fixed radiant uncertainty for the meteor (middle), and high-resolution model when assuming linear correlation between radiant uncertainty and velocity uncertainty (right). The gray line refers to the prior distribution, that is, the predicted ER ratios in the absence of orbital information or, equivalently, infinite orbital uncertainty. See Sect. 4.3 for a detailed discussion of these plots.



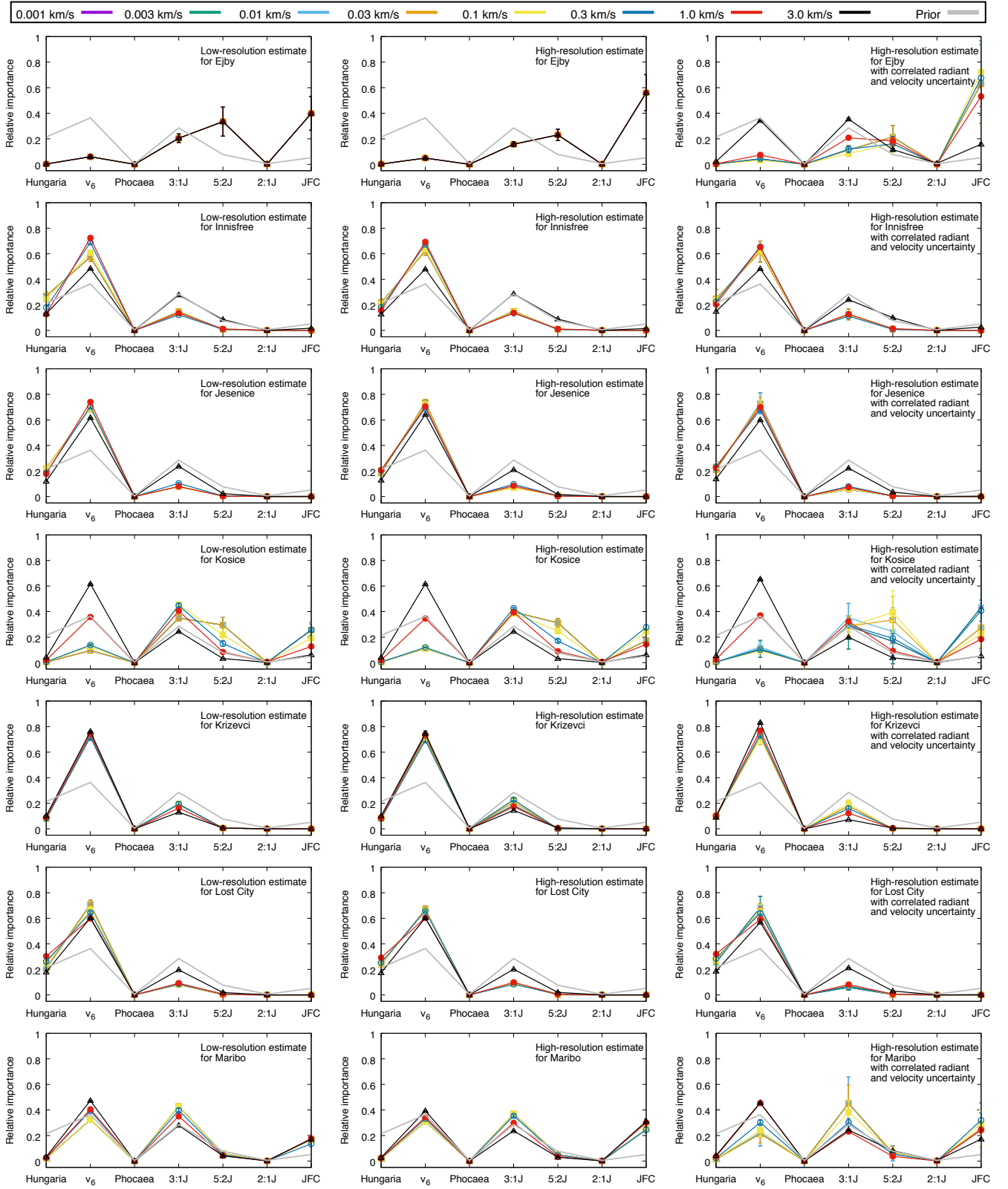


Figure 6: As Fig. 5.

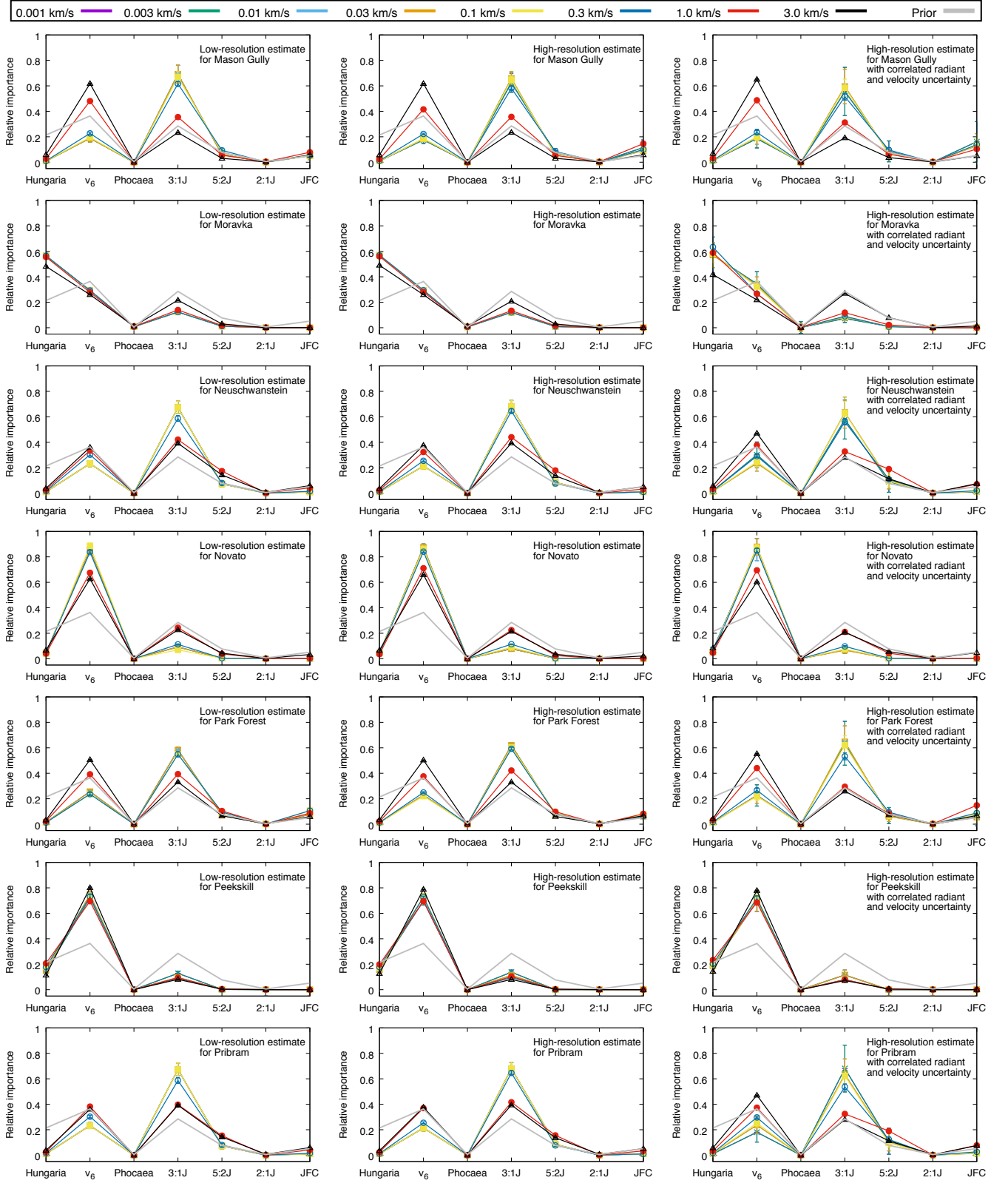


Figure 7: As Fig. 5.

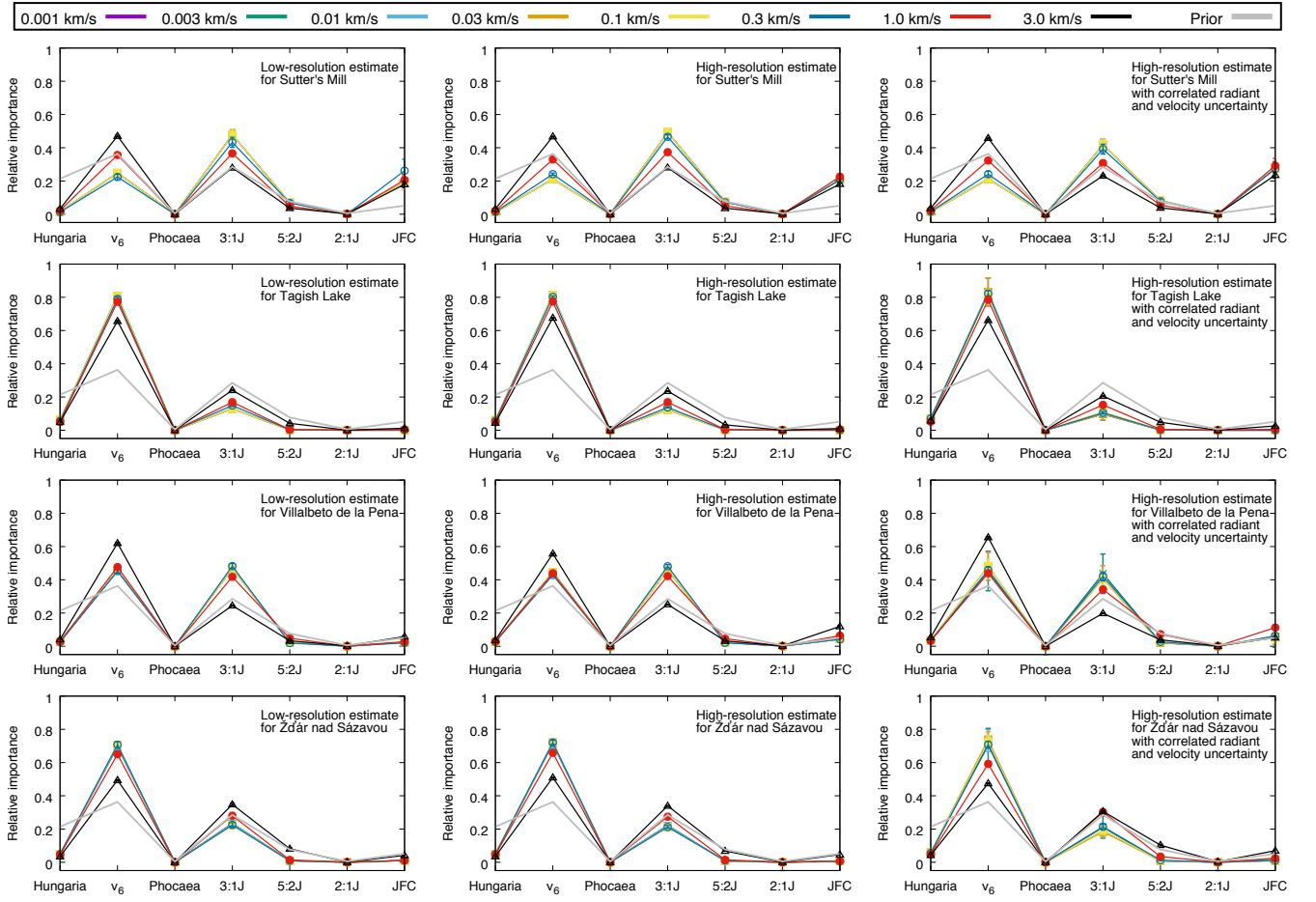


Figure 8: As Fig. 5.

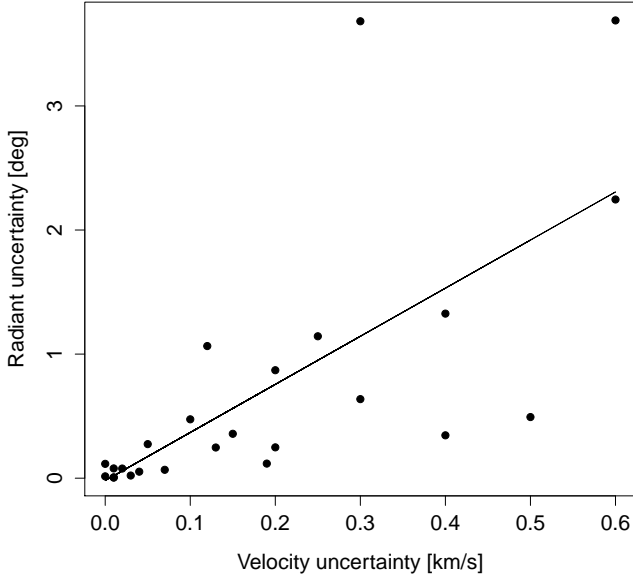


Figure 9: The observed correlation between velocity uncertainty and radiant uncertainty ( $\sqrt{(\Delta RA \cos(Dec))^2 + (\Delta Dec)^2}$ ) for meteorite-producing fireballs. The black line is a linear fit ( $y = ax + b$ ) to the data with  $a = (3.9 \pm 0.8)^\circ \text{ s km}^{-1}$  and  $b = (-0.02 \pm 0.22)^\circ$ .

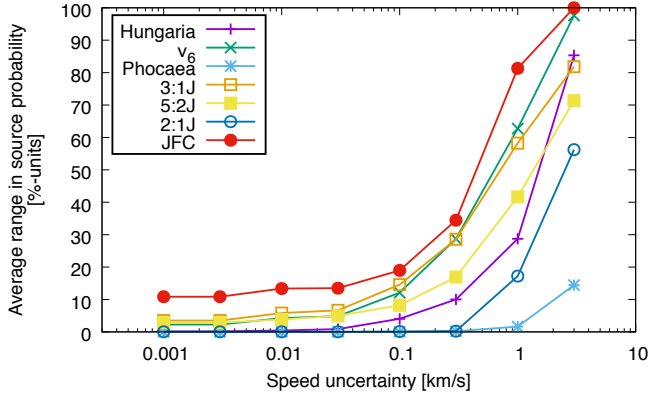


Figure 10: The average range in source probability as a function of uncertainty on measured meteor speed.

ilarly, increasing the resolution of the steady-state orbit distribution of the NEO model also had a limited effect on the uncertainties related to ER probabilities.

For the purpose of more accurately identifying meteorite ERs it would thus be more useful to increase the number of ERs that go into the NEO model rather than determining the meteoroid velocity more accurately or increasing the resolution of the NEO orbit model. That is, if the fairly extensive ER complexes used currently would be divided into their sub-components, it would become possible to provide more specific (but still probabilistic) estimates for the most likely ERs. Such an improvement primarily depends on the amount of NEO data available — the current choice to use 7 ERs in the state-of-the-art

NEO model is dictated by the need to ensure that the model is not degenerate (Granvik et al., 2016).

Finally, we may apply our results in terms of the optimal approaches to designing and operating fireball camera networks. In particular, our results suggest that a larger number of moderately precise meteorite recoveries, with speed precision of order a few hundred meters/sec will provide the most information regarding meteorite ERs and, ultimately, source regions.

## Acknowledgements

The authors wish to thank the two anonymous reviewers for their constructive suggestions that helped improve the paper. MG is grateful for the kind hospitality and financial support when visiting the University of Western Ontario’s Meteor Physics Group. MG acknowledges funding from the Academy of Finland (grant #299543) and the Ruth and Nils-Erik Stenbäck foundation. PGB was supported by funding from the Meteoroid Environment Office through NASA co-operative agreement NNX15AC94A, the Natural Sciences Research Council and the Canada Research Chairs program.

## References

- Baxter, M., Funkhouser, J., 1971. Lost City Meteorite Rare Gases in the Lost City and and Suchy Dul Meteorites. *Journal of Geophysical Research* 76.
- Binzel, R.P., Reddy, V., Dunn, T., 2015. The Near-Earth Object Population: Connections to Comets, Main-Belt Asteroids, and Meteorites, in: Michel, P., DeMeo, F.E., Bottke, W.F. (Eds.), *Asteroids IV*. University of Arizona Press. June 2015, pp. 243–256.
- Bischoff, A., Jersek, M., Grau, T., Mirtic, B., Ott, U., Kučera, J., Horstmann, M., Laubenstein, M., Herrmann, S., Randa, Z., Weber, M., Heusser, G., 2011. Jesenice-A new meteorite fall from Slovenia. *Meteoritics & Planetary Science* 46, 793–804.
- Bland, P., Spurný, P., Towner, M.C., Bevan, A., Singleton, A.T., Bottke, W., Greenwood, R.C., Chesley, S., Shrubny, L., Borovička, J., Ceplecha, Z., McClafferty, T.P., Vaughan, D., Benedix, G., Deacon, G., Howard, K.T., Franchi, I.A., Hough, R.M., 2009. An anomalous basaltic meteorite from the innermost main belt. *Science* 325, 1525–1527.
- Borovička, J., 2007. Properties of meteoroids from different classes of parent bodies, in: Milani, A., Valsecchi, G., Vokrouhlický, D. (Eds.), *Proceedings of IAU Symposium 236: Near Earth Objects, our celestial Neighbors: Opportunity and Risk*, Cambridge University Press, Cambridge, U.K.. p. 107.
- Borovička, J., Kalenda, P., 2003. The Morávka meteorite fall : 4 . Meteoroid dynamics and fragmentation in the atmosphere. *Meteorit. Planet. Sci.* 38, 1023–1043.
- Borovička, J., Popova, O., Nemtchinov, I., Spurný, P., Ceplecha, Z., 1998. Bolides produced by impacts of large meteoroids into the Earth’s atmosphere : comparison of theory with observations I. Benesov bolide dynamics and fragmentation. *Astronomy & Astrophysics* 334, 713–728.
- Borovička, J., Spurný, P., Brown, P., 2015a. Small Near-Earth Asteroids as a Source of Meteorites, in: *Asteroids IV*. 4th ed.. University of Arizona Press, pp. 257–280.
- Borovička, J., Spurný, P., Brown, P.G., Wiegert, P., Kalenda, P., Clark, D., Shrubny, L., 2013a. The trajectory, structure and origin of the Chelyabinsk asteroidal impactor. *Nature* 503, 235–237.

- Borovička, J., Spurný, P., Kalenda, P., Tagliaferri, E., 2003. The Morávka meteorite fall : 1. Description of the events and determination of the fireball trajectory and orbit from video records. *Meteorit. Planet. Sci.* 38, 975–987.
- Borovička, J., Spurný, P., Šegon, D., Andreić, Ž., Kac, J., Korlević, K., Atanackov, J., Kladnik, G., Mucke, H., Vida, D., Novoselnik, F., 2015b. The instrumentally recorded fall of the Križevci meteorite, Croatia, February 4, 2011. *Meteoritics & Planetary Science* 50, 1244–1259.
- Borovička, J., Tóth, J., Igaz, A., 2013b. The Košice meteorite fall: Atmospheric trajectory, fragmentation, and orbit. *Meteoritics & Planetary Science* 48, 1757–1779.
- Bottke, W.F., Morbidelli, A., Jedicke, R., Petit, J.M., Levison, H.F., Michel, P., Metcalfe, T.S., 2002. Debaised Orbital and Absolute Magnitude Distribution of the Near-Earth Objects. *Icarus* 156, 399–433.
- Britt, D.T., Consolmagno, G.J., 2003. Stony meteorite porosities and densities: A review of the data through 2001. *Meteoritics & Planetary Science* 38, 1161–1180.
- Brown, P., Wiegert, P., Clark, D., Tagliaferri, E., 2016. Orbital and physical characteristics of meter-scale impactors from airburst observations. *Icarus* 266, 96–111.
- Brown, P.G., Assink, J.D., Astiz, L., Blaauw, R., Boslough, M.B., Borovička, J., Brachet, N., Brown, D., Campbell-Brown, M., Cernanna, L., Cooke, W., de Groot-Hedlin, C., Drob, D.P., Edwards, W., Evers, L.G., Garces, M., Gill, J., Hedlin, M., Kingery, A., Laske, G., Le Pichon, A., Mialle, P., Moser, D.E., Saffer, A., Silber, E., Smets, P., Spalding, R.E., Spurný, P., Tagliaferri, E., Uren, D., Weryk, R.J., Whitaker, R., Krzeminski, Z., 2013. A 500-kiloton airburst over Chelyabinsk and an enhanced hazard from small impactors. *Nature* 503, 238–241.
- Brown, P.G., Ceplecha, Z., Hawkes, R., Wetherill, G., Beech, M., Mossman, K., 1994. The orbit and atmospheric trajectory of the Peekskill meteorite from video records. *Nature* 367, 624–626.
- Brown, P.G., McCausland, P., Fries, M., Silber, E., Edwards, W.N., Wong, D.K., Weryk, R., Fries, J., Krzeminski, Z., 2011. The fall of the Grimsby meteorite-I: Fireball dynamics and orbit from radar, video, and infrasound records. *Meteoritics & Planetary Science* 363, 339–363.
- Brown, P.G., Pack, D., Edwards, W.N., Revelle, D., Yoo, B.B., Spalding, R.E., Tagliaferri, E., 2004. The orbit, atmospheric dynamics, and initial mass of the Park Forest meteorite. *Meteorit. Planet. Sci.* 39, 1781–1796.
- Brown, P.G., ReVelle, D., Hildebrand, A., 2001. The Tagish Lake meteorite fall: interpretation of fireball physical characteristics, in: Warmbein, B. (Ed.), *Proceedings of the Meteoroids 2001 Conference*, European Space Agency, Noordwijk, The Netherlands. pp. 497–505.
- Brown, P.G., Revelle, D., Tagliaferri, E., Hildebrand, A., 2002. An entry model for the Tagish Lake fireball using seismic, satellite and infrasound records. *Meteorit. Planet. Sci.* 37, 661–676.
- Cartwright, J., Hermann, S., McCausland, P., Brown, P.G., Ott, U., 2010. Noble gas analysis of the Grimsby H chondrite, in: 73rd Meeting of the Meteoritical Society, New York. p. A30.
- Ceplecha, Z., 1961. Multiple fall of Pribram meteorites photographed. 1. Double-station photographs of the fireball and their relations to the found meteorites. *Bulletin of the Astronomical Institutes of Czechoslovakia* 12, 21–47.
- Ceplecha, Z., 1977. Fireballs photographed in central Europe. *Astronomical Institutes of Czechoslovakia, Bulletin* 28, 328–340.
- Ceplecha, Z., 1987. Geometric, dynamic, orbital and photometric data on meteoroids from photographic fireball networks. *Astronomical Institutes of Czechoslovakia, Bulletin* 38, 222–234.
- Ceplecha, Z., 1996. Luminous efficiency based on photographic observations of the Lost City fireball and implications for the influx of interplanetary bodies onto Earth. *Astronomy and Astrophysics* 311, 329–332.
- Ceplecha, Z., Brown, P.G., Hawkes, R., Wetherill, G., Beech, M., Mossman, K., 1996. Video observations, atmospheric path, orbit and fragmentation record of the fall of the Peekskill meteorite. *Earth, Moon and Planets* 72, 395–404.
- Ceplecha, Z., ReVelle, D., 2005. Fragmentation model of meteoroid motion, mass loss, and radiation in the atmosphere. *Meteoritics And Planetary Science* 40, 35–54.
- Clark, D., Wiegert, P., 2011. A numerical comparison with the Ceplecha analytical meteoroid orbit determination method. *Meteoritics & Planetary Science* 46, 1217–1225.
- Colas, F., 2016. Official launching of FRIPON. *eMeteorNews* 1, 67–68.
- de León, J., Pinilla-Alonso, N., Campins, H., Licandro, J., Marzo, G.A., 2012. Near-infrared spectroscopic survey of B-type asteroids: Compositional analysis. *Icarus* 218, 196–206.
- DeMeo, F.E., Carry, B., 2014. Solar System evolution from compositional mapping of the asteroid belt. *Nature* 505, 629–634.
- Dmitriev, V., Lupovka, V., Gritsevich, M., 2015. Orbit determination based on meteor observations using numerical integration of equations of motion. *PSS* 117, 223–235.
- Dunn, T.L., Burbine, T.H., Bottke, W.F., Clark, J.P., 2013. Mineralogies and source regions of near-Earth asteroids. *Icarus* 222, 273–282.
- Dyl, K.A., Benedix, G.K., Bland, P.A., Friedrich, J.M., Spurný, P., Towner, M.C., O’Keefe, M.C., Howard, K., Greenwood, R., Macke, R.J., Britt, D.T., Halfpenny, A., Thostenson, J.O., Rudolph, R.A., Rivers, M.L., Bevan, A.W., 2016. Characterization of Mason Gully (H5): The second recovered fall from the Desert Fireball Network. *Meteoritics and Planetary Science* 51, 596–613.
- Flynn, G.J., Consolmagno, G.J., Brown, P., Macke, R.J., 2017. Physical properties of the stone meteorites: Implications for the properties of their parent bodies. *Chemie der Erde - Geochemistry*, in press.
- Fry, C., Melanson, D., Samson, C., McCausland, P.J.A., Herd, R.K., Ernst, R.E., Umoh, J., Holdsworth, D.W., 2013. Physical characterization of a suite of Buzzard Coulee H4 chondrite fragments. *Meteoritics and Planetary Science* 48, 1060–1073.
- Gaffey, M.J., Gilbert, S., 1998. Asteroid 6 Hebe: The probable parent body of the H-type ordinary chondrites and the IIE iron meteorites. *Meteoritics & Planetary Science* 1295, 1281–1295.
- Gayon-Markt, J., Delbo, M., Morbidelli, A., Marchi, S., 2012. On the origin of the Almahata Sitta meteorite and 2008 TC<sub>3</sub> asteroid. *MNRAS* 424, 508–518.
- Goswami, J., Lal, D., Rao, M., Sinha, N., Venkatesan, T., 1978. Particle track and rare gas studies of Innisfree meteorite, in: (Meteoritical Society, Annual Meeting, 41st, Sudbury, Ontario, Canada, Aug. 14–17, 1978.) *Meteoritics*.
- Graf, T., Marti, K., Xue, S., Herzog, G.F., Klein, J., Middleton, R., Metzler, K., Herd, R., Brown, P., Wacker, J., Milton, B., Milton, J., 1997. Exposure history of the Peekskill (H6) meteorite. *Meteoritics* 32, 25–30.
- Granvik, M., Morbidelli, A., Jedicke, R., Bolin, B., Bottke, W.F., Beshore, E., Vokrouhlický, D., Delbò, M., Michel, P., 2016. Supercatastrophic disruption of asteroids at small perihelion distances. *Nature* 530, 303–306.
- Granvik, M., Morbidelli, A., Jedicke, R., Bolin, B., Bottke, W.F., Beshore, E., Vokrouhlický, D., Nesvorný, D., Michel, P., 2018. Debaised orbit and absolute-magnitude distributions for near-Earth objects. Accepted for publication in *Icarus*.
- Haak, H.W., Grau, T., Bischoff, A., Horstmann, M., Wasson, J., Sørensen, A., Laubenstein, M., Ott, U., Palme, H., Gellissen, M., Greenwood, R.C., Pearson, V.K., Franchi, I.A., Gabelica, Z., Schmitt-Kopplin, P., 2012. Maribo — A new CM fall from Denmark. *Meteoritics & Planetary Science* 47, 30–50.
- Haak, H.W., Michelsen, R., Stober, G., Keuer, D., Singer, W., 2010. The Maribo CM2 fall: radar based orbit determination of an unusually fast fireball, in: 73rd Meeting of the Meteoritical Society, p. 5085.
- Haak, H.W., Michelsen, R., Stober, G., Keuer, D., Singer, W., Williams, I.P., Unit, A., Mary, Q., Encke, C., 2011. CM Chondrites from Comets? - New Constraints from the orbit of the Maribo CM Chondrite Fall, in: *Formation of the First Solids in the Solar System*.
- Halliday, I., Blackwell, A., Griffin, A., 1978. The Innisfree meteorite

- and the Canadian camera network. *Royal Astronomical Society of Canada, Journal* 72, 15–39.
- Halliday, I., Griffin, A., Blackwell, A., 1981. The Innisfree meteorite fall- A photographic analysis of fragmentation, dynamics and luminosity. *Meteoritics* 16, 153–170.
- Halliday, I., Griffin, A., Blackwell, A., 1996. Detailed data for 259 fireballs from the Canadian camera network and inferences concerning the influx of large meteoroids. *Meteoritics and Planetary Science* 31, 185–217.
- Herzog, G., Caffee, M., 2014. 1.13 - Cosmic-Ray Exposure Ages of Meteorites. second edition ed.. Elsevier, Oxford. pp. 419 – 454.
- Hildebrand, A.R., McCausland, P.J.A., Brown, P.G., Longstaffe, F.J., Russell, S.D.J., Tagliaferri, E., Wacker, J.F., Mazur, M.J., Causland, P.J.A.M.C., 2006. The fall and recovery of the Tagish Lake meteorite. *Meteorit. Planet. Sci.* 41, 407–431.
- Horstmann, M., Bischoff, A., 2014. The Almahata Sitta polymict breccia and the late accretion of asteroid 2008 TC3. *Chemie der Erde - Geochemistry* 74, 149–183.
- Howie, R.M., Paxman, J., Bland, P.A., Towner, M.C., Cupak, M., Sansom, E.K., Devillepoix, H.A.R., 2017. How to build a continental scale fireball camera network. *Experimental Astronomy* 43, 237–266.
- Hutson, M., Ruzicka, A., Milley, E.P., Hildebrand, A., 2009. A first look at the petrography of the Buzzard Coulee (H4) chondrite, A recently observed fall from Saskatchewan, in: *Lunar and Planetary Science Conference (2009)*, p. 1893.
- Jenniskens, P., Fries, M.D., Yin, Q.Z., Zolensky, M., Krot, a.N., Sandford, S.a., Sears, D., Beauford, R., Ebel, D.S., Friedrich, J.M., Nagashima, K., Wimpenny, J., Yamakawa, a., Nishiizumi, K., Hamajima, Y., Caffee, M.W., Welten, K.C., Laubenstein, M., Davis, a.M., Simon, S.B., Heck, P.R., Young, E.D., Kohl, I.E., Thiemens, M.H., Nunn, M.H., Mikouchi, T., Hagiya, K., Ohsumi, K., Cahill, T.a., Lawton, J.a., Barnes, D., Steele, a., Rochette, P., Verosub, K.L., Gattacceca, J., Cooper, G., Glavin, D.P., Burton, a.S., Dworkin, J.P., Elsil, J.E., Pizzarello, S., Ogliore, R., Schmitt-Kopplin, P., Harir, M., Hertkorn, N., Verchovsky, a., Grady, M., Nagao, K., Okazaki, R., Takechi, H., Hiroi, T., Smith, K., Silber, E., Brown, P.G., Albers, J., Klotz, D., Hankey, M., Matson, R., Fries, J.a., Walker, R.J., Puchtel, I., Lee, C.T.a., Erdman, M.E., Eppich, G.R., Roeske, S., Gabelica, Z., Lerche, M., Nuevo, M., Girtten, B., Worden, S.P., 2012. Radar-Enabled Recovery of the Sutter's Mill Meteorite, a Carbonaceous Chondrite Regolith Breccia. *Science* 338, 1583–1587.
- Jenniskens, P., Rubin, A.E., Yin, Q.Z., Sears, D.W.G., Sandford, S.a., Zolensky, M.E., Krot, A.N., Blair, L., Kane, D., Utas, J., Verish, R., Friedrich, J.M., Wimpenny, J., Eppich, G.R., Ziegler, K., Verosub, K.L., Rowland, D.J., Albers, J., Gural, P., Grigsby, B., Fries, M.D., Matson, R., Johnston, M., Silber, E., Brown, P.G., Yamakawa, A., Sanborn, M.E., Laubenstein, M., Welten, K.C., Nishiizumi, K., Meier, M.M.M., Busemann, H., Clay, P., Caffee, M.W., Schmitt-Kopplin, P., Hertkorn, N., Glavin, D.P., Callahan, M.P., Dworkin, J.P., Wu, Q., Zare, R.N., Grady, M., Verchovsky, S., Emel'Yanenko, V., Naroenkov, S., Clark, D., Girtten, B., Worden, P.S., 2014. Fall, recovery, and characterization of the Novato L6 chondrite breccia. *Meteoritics & Planetary Science* 49, 1388–1425.
- Jenniskens, P., Shaddad, M.H., Numan, D., Elsir, S., Kudoda, A.M., Zolensky, M.E., Le, L., Robinson, G.A., Friedrich, J.M., Rumble, D., Steele, A., Chesley, S.R., Fitzsimmons, A., Duddy, S., Hsieh, H.H., Ramsay, G., Brown, P.G., Edwards, W.N., Tagliaferri, E., Boslough, M.B., Spalding, R.E., Dantowitz, R., Kozubal, M., Pravec, P., Borovicka, J., Charvat, Z., Vaubaillon, J., Kuiper, J., Albers, J., Bishop, J.L., Mancinelli, R.L., Sandford, S.A., Milam, S.N., Nuevo, M., Worden, S.P., 2009. The impact and recovery of asteroid 2008 TC3. *Nature* 458, 485–488.
- Kallemeyn, W., Rubin, A.E., Wang, D., Wasson, J.T., 1989. Ordinary chondrites: Bulk compositions, classification, lithophile-element fractionations, and composition-petrographic type relationships. *Geochimica et Cosmochimica Acta* 53, 2747–2767.
- Keuer D, S.W., G, S., 2009. Signatures of the ionization trail of a fireball observed in the HF, and VHF range above middle-Europe on January 17, 2009, in: *MST12 conference*, London, Ontario, May 17–23, 2009.
- Kohout, T., Donadini, F., Pesonen, L.J., Uehara, M., 2010. Rock magnetic studies of the Neuschwanstein EL6 chondrite - implications on the origin of its natural remanent magnetization. *Geophysica* 46, 3–19.
- Kohout, T., Gritsevich, M., Grokhovsky, V.I., Yakovlev, G.A., Haloda, J., Halodova, P., Michallik, R.M., Penttilä, A., Muinonen, K., 2014a. Mineralogy, reflectance spectra, and physical properties of the Chelyabinsk LL5 chondrite - Insight into shock-induced changes in asteroid regoliths. *Icarus* 228, 78–85.
- Kohout, T., Havrila, K., Tóth, J., Husárik, M., Gritsevich, M., Britt, D., Borovička, J., Spurný, P., Igaz, A., Svoreň, J., Kornoš, L., Vereš, P., Koza, J., Zigo, P., Gajdoš, Š., Világi, J., Čapek, D., Křišandová, Z., Tomko, D., Šilha, J., Schunová, E., Bodnárová, M., Búzová, D., Krejčová, T., 2014b. Density, porosity and magnetic susceptibility of the Košice meteorite shower and homogeneity of its parent meteoroid. *Planetary and Space Science* 93–94, 96–100.
- Kohout, T., Kiuru, R., Montonen, M., Scheirich, P., Britt, D.T., Macke, R., Consolmagno, G.J., 2011. Internal structure and physical properties of the Asteroid 2008 TC3 inferred from a study of the Almahata Sitta meteorites. *Icarus* 212, 697–700.
- Kohout, T., Meier, M.M.M., Maden, C., Busemann, H., Welten, K.C., Laubenstein, M., Caffee, M.W., Gritsevich, M., Grokhovsky, V., 2016. Pre-Entry Size and Cosmic History of the Annama Meteorite, in: *79th Annual Meeting of the Meteoritical Society*, p. 6316.
- Llorca, J., Guez, J.M.T.r., Ortiz, J.L., Docobo, J.A., Garcia-Guinea, J., Castro-Tirado, A.J., Rubin, A.E., Eugster, O., Edwards, W.N., Laubenstein, M., Casanova, I., 2005. The Villalbeto de la Peña meteorite fall : I . Fireball energy , meteorite recovery , strewn field , and petrography. *Meteoritics Planet. Sci.* 40, 795–804.
- Lyon, I., Andreic, Z., Segon, D., Korlevic, K., 2014. The Križevci H6 Chondrite and the Origin of H Chondrites, in: *77th Annual Meeting of the Meteoritical Society*, p. 5418.
- Macke, R., 2010. Survey of meteorite physical properties: density, porosity and magnetic susceptibility. Ph.D. thesis. University of Central Florida.
- McCausland, P., Brown, P., Hildebrand, A., Flemming, R., Barker, I., Moser, D., Renaud, J., Edwards, W.N., 2010. Fall of the Grimsby H5 Chondrite, in: *Lunar and Planetary Science Conference (2010)*.
- McCrosky, R., Posen, A., Schwartz, G., Shao, C.Y., 1971. Lost City Meteorites its Recovery and a Comparison with Other Fireballs. *Journal of Geophysical Research* 76, 4090–4108.
- Meier, M.M.M., Welten, K.C., Riebe, M.E.I., Caffee, M.W., Gritsevich, M., Maden, C., Busemann, H., 2017. Park Forest (L5) and the asteroidal source of shocked L chondrites. *Meteoritics & Planetary Science* 16.
- Milley, E.P., 2010. Physical Properties of fireball-producing earth-impacting meteoroids and orbit determination through shadow calibration of the Buzzard Coulee meteorite fall. Ph.D. thesis. University of Calgary.
- Milley, E.P., Hildebrand, A., Brown, P.G., Noble, M., Sarty, G., Ling, A., Mailler, L., 2010. Pre-fall Orbit of the Buzzard Coulee Meteoroid, in: *Geocanada 2010 - Working with the Earth*, p. 4.
- Morbidelli, A., Gladman, B., 1998. Orbital and temporal distributions of meteorites originating in the asteroid belt. *Meteoritics and Planetary Science* 33, 999–1016.
- Nava, D., Walter, L.S., Doan, A., 1971. Chemistry and Mineralogy of the Lost City Meteorite. *Journal of Geophysical Research* 76, 4067–4071.
- Nesvorný, D., Vokrouhlický, D., Morbidelli, A., Bottke, W., 2009. Asteroidal source of L chondrite meteorites. *Icarus* 200, 698–701.
- Nishiizumi, K., Caffee, M.W., Hamajima, Y., Reedy, R.C., Welten, K.C., 2014. Exposure history of the Sutter's Mill carbonaceous chondrite. *Meteoritics & Planetary Science* 49, 2056–2063.
- Novaković, B., Tsirvoulis, G., Granvik, M., Todović, A., 2017. A Dark Asteroid Family in the Phocaea Region. *Astronomical Journal* 153, 266.

- Ozdín, D., Plavčan, J., Horňáčková, M., Uher, P., Porubčan, V., Veis, P., Rakovský, J., Tóth, J., Konečný, P., Svoreň, J., 2015. Mineralogy, petrography, geochemistry, and classification of the Košice meteorite. *Meteoritics & Planetary Science* 50, 864–879.
- Pauls, A., Gladman, B., 2005. Decoherence Time Scales for Meteoroid Streams. *Meteoritics and Planetary Science* 40, 1241–1256.
- Popova, O.P., Jenniskens, P., Emel'yanenko, V., Kartashova, A., Biryukov, E., Khaibrakhmanov, S., Shuvalov, V., Rybnov, Y., Dudorov, A., Grokhovsky, V.I., Badyukov, D.D., Yin, Q.Z., Gural, P.S., Albers, J., Granvik, M., Evers, L.G., Kuiper, J., Kharlamov, V., Solovyov, A., Rusakov, Y.S., Korotkiy, S., Serdyuk, I., Korochantsev, A.V., Larionov, M.Y., Glazachev, D., Mayer, A.E., Gislér, G., Gladkovsky, S.V., Wimpenny, J., Sanborn, M.E., Yamakawa, A., Verosub, K.L., Rowland, D.J., Roeske, S., Botto, N.W., Friedrich, J.M., Zolensky, M.E., Le, L., Ross, D., Ziegler, K., Nakamura, T., Ahn, I., Lee, J.I., Zhou, Q., Li, X.H., Li, Q.L., Liu, Y., Tang, G.Q., Hiroi, T., Sears, D., Weinstein, I.A., Vokhmintsev, A.S., Ishchenko, A.V., Schmitt-Kopplin, P., Hertkorn, N., Nagao, K., Haba, M.K., Komatsu, M., Mikouchi, T., t.C.j..S.y..m..n.v..p...a.h.a..P., .
- Povinec, P.P., Masarik, J., Sýkora, I., Kováčik, A., Beňo, J., Meier, M.M., Wieler, R., Laubenstein, M., Porubčan, V., 2015. Cosmogenic nuclides in the Košice meteorite: Experimental investigations and Monte Carlo simulations. *Meteoritics and Planetary Science* 50, 880–892.
- Pravec, P., Harris, A.W., Kušnirák, P., Galád, A., Hornoch, K., 2012. Absolute magnitudes of asteroids and a revision of asteroid albedo estimates from WISE thermal observations. *Icarus* 221, 365–387.
- Righter, K., Abell, P., Agresti, D., Berger, E.L., Burton, A.S., Delaney, J.S., Fries, M.D., Gibson, E.K., Haba, M.K., Harrington, R., Herzog, G.F., Keller, L.P., Locke, D., Lindsay, F.N., McCoy, T.J., Morris, R.V., Nagao, K., Nakamura-Messenger, K., Niles, P.B., Nyquist, L.E., Park, J., Peng, Z.X., Shih, C.Y., Simon, J.I., Swisher, C.C., Tappa, M.J., Turrin, B.D., Zeigler, R.A., 2015. Mineralogy, petrology, chronology, and exposure history of the Chelyabinsk meteorite and parent body. *Meteoritics and Planetary Science* 50, 1790–1819.
- Rivkin, A.S., 2012. The fraction of hydrated C-complex asteroids in the asteroid belt from SDSS data. *Icarus* 221, 744–752.
- Rubin, A.E., 1990. Kamacite and olivine in ordinary chondrites - Intergroup and intragroup relationships. *Geochimica et Cosmochimica Acta* 54, 1217–1232.
- Schunová, E., Granvik, M., Jedicke, R., Gronchi, G., Wainscoat, R., Abe, S., 2012. Searching for the first near-Earth object family. *Icarus* 220, 1050–1063.
- Simon, S., Grossman, L., Clayton, R.N., Mayeda, T., Schwade, J., Sipiera, P., Wacker, J., Wadhwa, M., 2004. The fall, recovery, and classification of the Park Forest meteorite. *Meteoritics & Planetary Science* 39, 625–634.
- Smith, D.G.W., 1980. The mineral chemistry of the innisfree meteorite. *The Canadian Mineralogist* 18, 433–442.
- Spurný, P., 1994. Recent fireballs photographed in central Europe. *Planetary and Space Science* 42, 157–162.
- Spurný, P., 2015. Instrumentally documented meteorite falls: two recent cases and statistics from all falls. *Proceedings of the International Astronomical Union* 10, 69–79.
- Spurný, P., Bland, P., Borovička, J., Towner, M., Shrbený, L., Bevan, A., Vaughan, D., 2012b. The Mason Gully meteorite fall in SW Australia: Fireball Trajectory, Luminosity, Dynamics, Orbit and Impact Position from photographic records, in: *Asteroids Comets Meteors 2012*, p. 6369.
- Spurný, P., Bland, P., Shrbený, L., Borovička, J., Cepelcha, Z., Singelton, A., Bevan, A.W.R., Vaughan, D., Towner, M.C., McClafferty, T.P., Touni, R., Deacon, G., 2012a. The Bunburra Rockhole meteorite fall in SW Australia: fireball trajectory, luminosity, dynamics, orbit, and impact position from photographic and photoelectric records. *Meteoritics & Planetary Science* 47, 163–185.
- Spurný, P., Borovička, J., Baumgarten, G., Haack, H., Heinlein, D., Sørensen, A., 2016a. Atmospheric trajectory and heliocentric orbit of the Ejby meteorite fall in Denmark on February 6, 2016. *Planetary and Space Science* .
- Spurný, P., Borovička, J., Haack, H., Singer, W., Keuer, D., Jobse, K., 2013. Trajectory and Orbit of the Maribo CM2 Meteorite from optical, photoelectric and radar records, in: *Meteoroids 2013*.
- Spurný, P., Borovička, J., Haloda, J., Shrbený, L., Heinlein, D., 2016b. Two very precisely instrumentally documented meteorite falls: Zdar nad Sazavou and Stubenberg - Prediction and Reality, in: 79th Meteoritical Society Meeting, p. 6221.
- Spurný, P., Borovička, J., Kac, J., Kalenda, P., Atanackov, J., Kladnik, G., Heinlein, D., Grau, T., 2010. Analysis of instrumental observations of the Jesenice meteorite fall on April 9, 2009. *Meteoritics & Planetary Science* 45, 1392–1407.
- Spurný, P., Borovička, J., Shrbený, L., 2007. Automation of the Czech part of the European fireball network: equipment, methods and first results. *Proceedings of the International Astronomical Union* 2, 121–131.
- Spurný, P., Haloda, J., Borovička, J., Shrbený, L., Halodová, P., 2014. Reanalysis of the Benešov bolide and recovery of polymict breccia meteorites — old mystery solved after 20 years. *Astronomy & Astrophysics* 570, A39.
- Spurný, P., Heinlein, D., Oberst, J., 2002. The atmospheric trajectory and heliocentric orbit of the Neuschwanstein meteorite fall on April 6, 2002, in: *Asteroids, Comets, and Meteors: ACM 2002*, pp. 137–140.
- Spurný, P., Oberst, J., Heinlein, D., 2003. Photographic observations of Neuschwanstein , a second meteorite from the orbit of the Příbram chondrite. *Nature* 423, 151–3.
- Stauffer, H., Urey, H., 1962. Multiple fall of Příbram meteorites photographed. III. Rare gas isotopes in the Velká stone meteorite. *Bulletin of the Astronomical Institutes of Czechoslovakia* 13, 106.
- Tancredi, G., 2014. A criterion to classify asteroids and comets based on the orbital parameters. *Icarus* 234, 66–80.
- Trigo-Rodríguez, J., Borovička, J., Spurný, P., Ortiz, J.L., Docobo, J.A., Castro-Tirado, A.J., Llorca, J., 2006. The Villalbeto de la Peña meteorite fall: II. Determination of atmospheric trajectory and orbit. *Meteorit. Planet. Sci.* 41, 505–517.
- Trigo-Rodríguez, J.M., Lyytinen, E., Gritsevich, M., Moreno-Ibáñez, M., Bottke, W.F., Williams, I., Lupovka, V., Dmitriev, V., Kouchout, T., Grokhovsky, V., 2015. Orbit and dynamic origin of the recently recovered Annama's H5 chondrite. *MNRAS* 449, 2119–2127.
- Tucek, K., 1961. Multiple fall of příbram meteorites photographed 2. Morphological and mineralogical composition of the meteoritic stones of příbram. *Bulletin of the Astronomical Institutes of* .
- Vernazza, P., Binzel, R.P., Thomas, C.A., DeMeo, F.E., Bus, S.J., Rivkin, A.S., Tokunaga, A.T., 2008. Compositional differences between meteorites and near-Earth asteroids. *Nature* 454, 858–860.
- Vernazza, P., Marsset, M., Beck, P., Binzel, R.P., Birlan, M., Cloutis, E.A., DeMeo, F.E., Dumas, C., Hiroi, T., 2016. Compositional Homogeneity of CM Parent Bodies. *AJ* 152, 54.
- Vokrouhlický, D., Farinella, P., 2000. Efficient delivery of meteorites to the Earth from a wide range of asteroid parent bodies. *Nature* 407, 606–8.
- Welten, K.C., Meier, M.M.M., Caffee, M.W., Laubenstein, M., Nishiizumi, K., Wieler, R., Bland, P., Towner, M.C., Spurný, P., 2012. Cosmic-ray exposure age and preatmospheric size of the Bunburra Rockhole achondrite. *Meteoritics & Planetary Science* 47, 186–196.
- Welten, K.C., Meier, M.M.M., Caffee, M.W., Nishiizumi, K., Wieler, R., Jenniskens, P., Shaddad, M.H., 2010. Cosmogenic nuclides in Almahata Sitta ureilites: Cosmic-ray exposure age, preatmospheric mass, and bulk density of asteroid 2008 TC3. *Meteoritics & Planetary Science* 45, 1728–1742.
- Wetherill, G., 1985. Asteroidal source of ordinary chondrites. *Meteoritics* 20, 1–22.
- Wetherill, G., ReVelle, D., 1982. Relationships between comets, large meteors, and meteorites. *Comets*, University of Arizona Press, Tucson, AZ, USA , 297–319.
- Wisdom, J., 2017. Meteorite transport - Revisited. *Meteoritics & Planetary Science* 52, 1660–1668.
- Wlotzka, F., 1993. The Meteoritical Bulletin, No 75, 1993 December.

Meteoritics 28, 692–703.

Zipfel, J., Bischoff, A., Schultz, L., Spettel, B., Dreibus, G., Schönbeck, T., Palme, H., 2010. Mineralogy, chemistry, and irradiation record of Neuschwanstein (EL6) chondrite. *Meteoritics and Planetary Science* 45, 1488–1501.

Zolensky, M., Mikouchi, T., Fries, M., Bodnar, R., Jenniskens, P., Yin, Q.z., Hagiya, K., Ohsumi, K., Komatsu, M., Colbert, M., Hanna, R., Maisano, J., Ketcham, R., Kebukawa, Y., Nakamura, T., Matsuoka, M., Sasaki, S., Tsuchiyama, A., Gounelle, M., Le, L., Martinez, J., Ross, K., Rahman, Z., 2014. Mineralogy and petrography of C asteroid regolith: The Sutter's Mill CM meteorite. *Meteoritics & Planetary Science* 49, 1997–2016.